International Journal of Solids and Structures 88–89 (2016) 337–353

Contents lists available at ScienceDirect

International Journal of Solids and Structures

journal homepage: www.elsevier.com/locate/ijsolstr

Impact perforation of polymer–metal laminates: Projectile nose shape sensitivity

I. Mohagheghian, G.J. McShane*, W.J. Stronge

Department of Engineering, University of Cambridge, Trumpington Street, Cambridge CB2 1PZ, UK

ARTICLE INFO

Article history:
Received 13 October 2015
Revised 16 December 2015
Available online 23 January 2016

Keywords:
Polymer metal bi-layer
Perforation
Projectile nose shape

ABSTRACT

Recent research has established that polymer–metal laminates are able to provide enhanced impact perforation resistance compared to monolithic metallic plates of the same mass. A number of mechanisms have been proposed to explain this benefit, including the dissipation of energy within the polymer itself, and the polymer deformation enhancing dissipation within the metallic layer. This understanding of the layer interactions and synergies informs the optimisation of the laminate. However, the effect of the nose shape geometry of the projectile on perforation resistance of a particular laminate configuration has not been established. An optimal laminate configuration for one projectile may be sub-optimal for another. This investigation aims to clarify this nose shape sensitivity for both the quasi-static and impact perforation resistance of light-weight polymer–metal laminates. Bi-layer plates are investigated, with a polyethylene layer positioned on either the impacted or distal face of a thin aluminium alloy substrate. Three contrasting nose shapes are considered: blunt, hemi-spherical and conical. These have been shown to induce distinctly different deformation and fracture modes when impacting monolithic metallic targets. For all projectile nose shapes, placing a polyethylene layer on the impacted (rather than distal) face of the bi-layer plate results in an increase in perforation resistance compared to the bare substrate, by promoting plastic deformation in the metal backing. However, the effectiveness of the polymer in enhancing perforation resistance is sensitive to both the thickness of the polymer layer and the nose shape of the projectile. For a thin polyethylene layer placed on the impacted face, the perforation resistance is greatest for the blunt projectile, followed by the hemi-spherical and conical nose geometries. As the thickness of the polymer facing layer approaches the projectile radius, there is a convergence in both failure mode and perforation energy for all three nose shapes. Bi-layer targets can outperform monolithic metallic targets on an equal mass basis, though this is sensitive to the type of polyethylene used, the polymer layer thickness and the projectile nose shape. The greatest benefit of bi-layer construction (on an equal mass basis) is seen for blunt projectiles, using a polyethylene that maintains a high degree of strain hardening at high strain rates (i.e. UHMWPE), and a polymer thickness just sufficient to switch the failure mode in the metal layer from discing (failure at the projectile perimeter) to tensile failure at the plate centre.

1. Introduction

There is currently a growing interest in using polymer coatings to enhance the impact and blast resistance of structural panels (Mock et al., 2005; Roland et al., 2010; Barsoum and Dudt, 2010; Amini et al., 2010a, 2010b). Polymers such as polyurea can be easily applied as a coating to a variety of surfaces, from masonry walls to armoured vehicles, curing rapidly in-situ at room temperature. This is an attractive solution for retro-fitting to enhance resilience. Recent studies have shown promising results for such polymer coatings. However, to date, much of this work has focussed on blast loading. Investigations into the influence of a polymer coating on the resistance to projectile perforation of a target plate remain relatively limited.

It has been shown by Mohagheghian et al., in press that a polymer layer can significantly enhance the impact perforation resistance of a thin metallic plate struck by a blunt-nosed projectile. When placed on the impacted (proximal) face, the polymer deforms under the projectile, altering its effective tip geometry and increasing plastic deformation in the metallic substrate. It was shown that the thickness of the polymer layer can be chosen such that it maximises this effect, optimising the perforation resistance.

* Corresponding author. Tel.: +44 1223 332635.
E-mail address: gjm31@cam.ac.uk (G.J. McShane).

http://dx.doi.org/10.1016/j.ijsolstr.2016.01.010

However, it is not clear how sensitive the ideal laminate configuration is to the tip geometry of the projectile. The current investigation will address this issue.

The projectile nose shape sensitivity of the projectile perforation resistance of monolithic metallic plates has been extensively investigated (Corran et al., 1983; Leppin and Woodward, 1986; Børvik et al., 2002; Gupta et al., 2007; Iqbal et al., 2010). It has been established that different nose shapes can induce very different deformation and failure mechanisms in the metallic target. This nose shape sensitivity is also dependent on the thickness of the target and velocity of the projectile. For a blunt projectile impacting thin metallic plates, failure is by plugging, resulting in a disc-shaped fragment with diameter equal to that of the projectile detaching from the target (Palomby and Stronge, 1988). For a hemi-spherical nosed projectile, circumferential fracture of the plate causes a spherical cap of diameter less than that of the projectile to detach, followed by enlargement of the resulting hole as penetration continues to full perforation of the target. If the material has low ductility, this hole enlargement causes some radial cracking and the formation of symmetric petals. For a conical projectile failure proceeds through petalling and petal bending. The number of petals depends on the cone angle of the nose, as well as the material properties of the target (Atkins et al., 1998). For all three projectile geometries, the plate deforms plastically before the onset of fracture. Plastic deformation modes include bulging (the local deformation of the plate below the indenter) and dishing (the global deformation of the target which can extend a considerable distance from the impact area) (Backman and Goldsmith, 1978). The level of dishing in the plate also depends on the projectile nose shape. It is greatest for a hemi-spherical nose, followed by blunt and then conical.

The performance of multi-layer metallic targets is also affected by the nose shape of the projectile. Teng et al. (2007) numerically analysed the impact performance of a bi-layer target, each layer having the same material and thickness, and compared it with an equal mass monolithic plate. They found that the layered configuration can increase the ballistic limit by up to 25% for a blunt projectile. However, for a conical projectile the performance of the bi-layer is nearly the same as the monolithic plate. In a separate study, Teng et al. (2008) numerically investigated the impact response of metallic bi-layers with dissimilar layer properties. Relative to monolithic targets, the performance of the bi-layers was dependent on both the nose shape and the order of the layers.

Most of the studies performed to date on the impact response of polymer–metal bi-layer targets have focussed on a single projectile nose shape. Roland et al. (2010, 2013) investigated the performance of an elastomer–steel laminate impacted by fragment-simulating projectiles (a relatively blunt geometry). The polymer was placed on the impacted face. They argued that an impact-induced transition of the polymer to a glassy state is a key factor in the observed improvement in the ballistic limit for this scenario. Radin and Goldsmith (1988) investigated the performance of a polymer–metal bi-layer consisting of aluminium alloy and polycarbonate layers impacted by a conical projectile. They found that the bi-layer outperforms a monolithic metal plate of the same areal density, but underperforms the same weight of monolithic polymer. They suggested that placing metal on the impacted face is more effective for a conical projectile. It was observed that the penetration mode in the aluminium plate changed from petalling to cratering (extrusion of material at the periphery of the projectile which can form lips on both the distal and proximal face) when the aluminium plate was supported by a thick polycarbonate backing. Low-velocity drop-weight impact tests were conducted by Liu and Liaw (2009) on PMMA-aluminium bi-layers with an epoxy adhesive interface. In contrast to (Radin and Goldsmith, 1988), their experiments showed that the impact damage (including delamination, and fracture of the polymer plate) is more severe when the aluminium plate is located on the impacted face. They argued that delamination of the interface occurs sooner when the thinner and less stiff layer (the metal layer in this case) is located on the impacted face. As noted above, for light-weight polymer–metal bi-layer plates loaded by a blunt indenter, Mohagheghian et al., in press found significant improvement in perforation energy when the polymer was located on the impacted face. However, the sensitivity of the observed perforation mechanisms to the geometry of the impacting projectile was not identified.

The only previous investigation identified by the authors that has systematically compared the impact performance of a polymer–metal bi-layer plate for different projectile nose shapes was conducted by Xue et al. (2010). Their numerical results suggest that placing a polyurea backing on the distal face of a steel plate is more effective against impacts by a conical projectile, and rather less effective for a blunt projectile (42% and 13% improvement relative to the bare substrate, respectively). They argued that for a conical projectile, the energy absorption in the metal layer is increased with the addition of a polymer coating due to a delay in the onset of fracture of the steel plate. However, for the blunt projectile the polyurea backing decreases the energy absorbed by the steel layer, with the overall performance benefit due to the additional energy dissipated in polymer deformation.

Although the study of Xue et al. (2010) begins to address the question of nose shape sensitivity, only a small range of target and impact configurations were considered, and a number of questions remain to be answered. The effect of (i) the order of the layers relative to the loading direction, (ii) material properties and (iii) the thickness of the polymer layer on the impact performance as well as (iv) their relative performance in comparison with equal mass monolithic targets (both metal and polymer) has not been established. These questions form the focus of the present investigation.

1.1. Outline of the investigation

The aim of this investigation is to determine how the impact perforation mechanisms and synergies between layers reported by Mohagheghian et al., in press for light-weight bi-layer plates are influenced by the nose shape of the projectile. The target configurations are similar to those of Mohagheghian et al., in press: laminated plates consisting of one polymer and one thin metallic layer. Three distinct nose shapes are considered: blunt (flat nosed circular cylinder), hemi-spherical and conical (with a cone angle of 90°). These are chosen as they have been shown to induce contrasting deformation and failure mechanisms in monolithic metallic targets. The influence of the order of the layers, as well as the thickness and properties of the polymer layer in the bi-layer target are considered. The strategy adopted in this investigation is similar to that of Mohagheghian et al., in press First the quasi-static perforation of the plates is considered, in order to gain a clear insight into the modes of deformation and failure in the absence of significant inertia and strain rate effects. Next, the impact perforation of the targets is considered, and interpreted in light of the findings from the quasi-static tests.

2. Test methodology and specimen configuration

The test specimens used in this investigation consist of flat plates with a circular target area fully clamped around the edge at a radius $R = 50$ mm. The boundary condition is provided by a circular steel clamping ring with inner diameter 100 mm, as shown in Fig. 1a. Twelve M4 bolts are used to fasten the clamping ring through clearance holes in the test specimen (a square plate of side length 130 mm) to a supporting plate. Three distinct nose shapes are used for the projectiles in the impact tests and the indenters

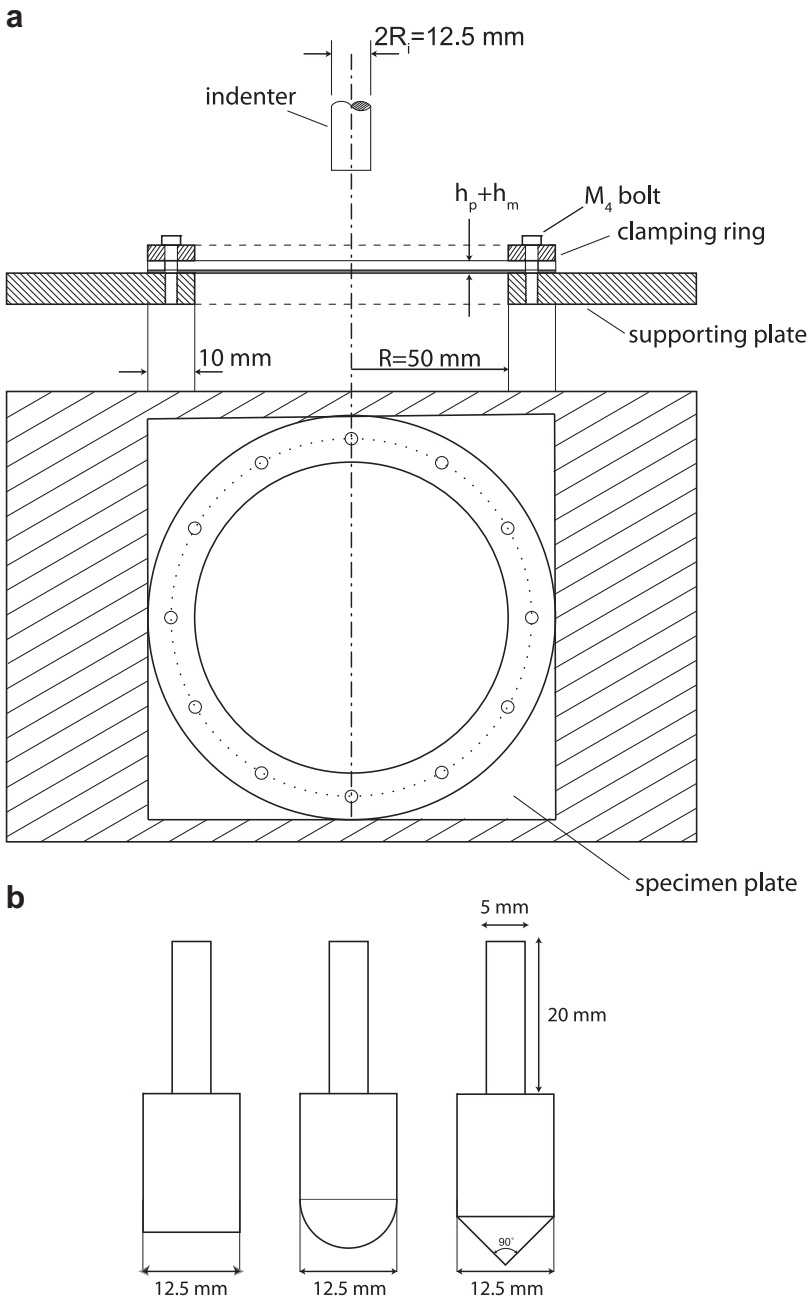

Fig. 1. Schematic of (a) plate clamping arrangement and (b) indenter geometries.

in the quasi-static experiments, each with diameter 12.5 mm, as shown in Fig. 1b. The ratio of the projectile (or indenter) radius to the plate radius is therefore $R_I/R = 0.125$. The projectiles and indenters are machined from mild steel, and undergo no plastic deformation during the experiments.

Aluminium alloy 6082-T6 is used for the metallic substrate of the polymer–metal bi-layer and for the monolithic metal targets. We use polyethylene (PE) for the polymer layer. Polyethylenes are available with a range of mechanical properties, without significantly altering the material density. Thus, polyethylene/aluminium laminates provide a convenient model system for systematic investigation of the bi-layer response. The details of the materials used in this study are listed in Table 1.

2.1. Quasi-static perforation experiments

The quasi-static perforation experiments were performed using an Instron screw driven test machine. The indenters were mounted to the load cell on the cross-head of the test machine with the specimen and clamping plate beneath. The load cell was used to provide the indentation force and the cross-head displacement gave the indentation distance. Separate tests confirmed that, for the plate specimens tested here, cross-head compliance has a negligible influence on the measurements. The perforation tests were stopped after the indenter had fully perforated all layers. The quasi-static tests were conducted at an indenter speed of 1 mm min^{-1}.

Table 1
Specification of the materials used in this study.

Material	Product name	Density (kg m^{-3})	Thickness (mm)	Yield strength (MPa)***	Nominal failure strain (–)***
AA 6082 T6	L113*	2700	1.0	302.4	0.16
LDPE	LDPE—Natural**	930	3.0	11.9	7.2
HDPE	HD-PE300—Natural**	960	2.9	27.6	21.7
UHMWPE	UHMW-PE1000—Natural**	940	3.0	22.0	10.1

* Supplied by: Smiths Metal Centres Ltd, Biggleswade, Bedfordshire, UK.
** Supplied by: Engineering & Design Plastics Ltd, Cambridge, UK.
*** Average values obtained at the strain rate of 0.001 s^{-1} (Mohagheghian et al., 2015).

2.2. Impact perforation experiments

Projectile impact tests were conducted using identical plate geometry and boundary conditions to the quasi-static tests (as shown in Fig. 1a). Projectiles with the three nose shapes (blunt, hemispherical and conical) were fired using a gas gun apparatus. The projectiles were machined so as to keep their masses constant at $m = 20.2 \pm 0.2$ g. In order to measure the initial velocity of the projectile, laser velocity gauges were mounted at the end of the gas gun barrel. A high speed camera was also used to record the position of the projectile as a function of time throughout the impact at a rate of 23,000 frames per s. As shown in Fig. 1b, the projectiles were machined with a tail section of length 20 mm and diameter 5 mm, to allow the position to be tracked when the main body of the projectile is obscured by the target and clamping ring. The high speed photography was used to calculate both the impact velocity (to confirm the measurements from the laser velocity gauge) and the residual velocity.

In order to determine the ballistic limit, experiments were performed at a number of impact velocities both above and below that required for full perforation. Plotting residual velocity against impact velocity, a curve based on the Lambert and Jonas relation (Lambert and Jonas, 1976) was fitted to the data points for which full perforation occurred (i.e. for which there was a positive residual velocity). The coincidence of this curve with the impact velocity axis is taken to be the ballistic limit. To improve the resolution of the measurement, after a first estimate was obtained, at least four impact experiments were conducted within an impact velocity range of $\pm$ 4 m s^{-1} of the ballistic limit. Details of the impact versus residual velocity curves are given in the Appendix.

3. Nose shape sensitivity: monolithic metal target

The nose-shape sensitivity of the perforation of monolithic metallic targets, which use the same Al alloy as the bi-layer specimens, is first considered. This provides a reference case against which to compare the bi-layer results. Aluminium alloy 6082-T6 is used with a plate thickness $h_m = 1$ mm. In order to characterise the material, nominal tensile stress–strain curves were obtained using dog-bone specimens with geometry following ASTM-E8 (ASTM E8/E8m-11, 2011) (the gauge section has length 32 mm and width 6 mm) machined from identical sheet material. The result is plotted in Fig. 2a. The 6082-T6 has a yield strength of approximately 300 MPa, and fails at around 16% nominal tensile strain. Measurements from specimens oriented either parallel or perpendicular to the rolling direction of the sheet showed that the material is isotropic in-plane.

3.1. Quasi-static perforation of monolithic metallic plates

The quasi-static indentation response of monolithic aluminium alloy plates is shown in Fig. 3 for the three indenter nose shapes. In each case, the response is divided into two phases. We denote phase I as the response up until failure initiates in the metal, identified by the first load drop in the force–displacement curve. [1] During this phase, energy is absorbed mainly through plastic bending and stretching of the plate. Phase II is the response after the initiation of failure in the metal. Comparing the three nose shapes during phase I, two factors influence the total energy absorption: the slope of the force–displacement curve and the indenter displacement at the onset of fracture (the end of phase I). The former can be linked to the area of plate loaded by the indenter, as analysed by Onat and Haythornthwaite (Onat and Haythornthwaite, 1954). A larger loading patch size (as is the case for the blunt tip,

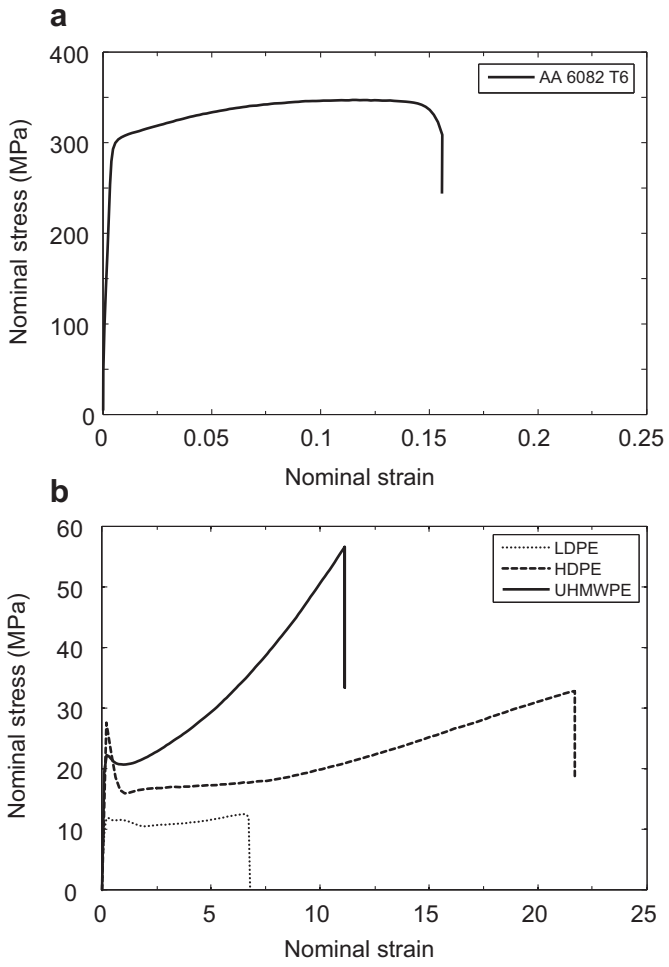

Fig. 2. Quasi-static tensile response of: (a) Al alloy 6082-T6, (b) polyethylenes LDPE, HDPE and UHMWPE.

[1] Some small-scale local penetration of the plate is observed for the sharp-tipped conical projectile earlier in the response. However, for consistency, we define the end of phase I in this case to be the first load drop, which is the point at which significant fracture of the metal target plate first occurs.

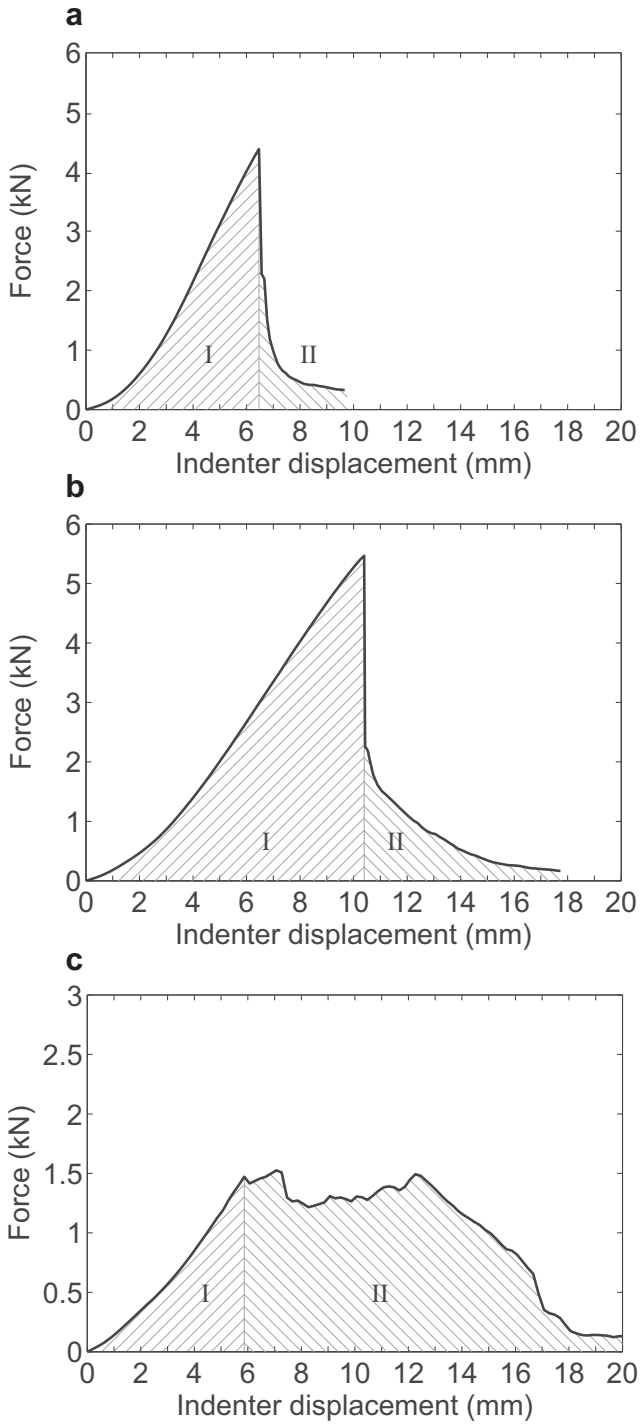

Fig. 3. Quasi-static indentation response of a monolithic Al alloy plate ($h_m = 1$ mm) loaded by (a) blunt, (b) hemi-spherical and (c) conical indenters. The indentation force and indenter displacement are F and u_I, respectively.

versus the hemi-spherical or conical) leads to a larger gradient. Simple analytical expressions able to accurately predict the indenter displacement at the onset of fracture for different nose shapes are however unavailable, due to its complex dependence on the evolving state of stress in the plate. These complexities have also been recognised in metal forming applications; e.g. deep drawing and stretch bending, using different tool sizes (Li et al., 2010; Luo and Wierzbicki, 2010).

The experiments show that a plate loaded by the conical indenter fails at the smallest indenter displacement, with failure in this case initiated by the formation of four symmetric cracks and the detachment of a small circular cap at the indenter tip. Next is the blunt indenter, with failure occurring by plugging: fracture that develops around the perimeter of the indenter, detaching a circular disc. The largest indenter displacement at failure is achieved using a hemi-spherically nosed indenter. Here, a circumferential crack occurs at the tip of the indenter, detaching a circular cap of radius slightly less than that of the indenter. For the hemi-spherical indenter, failure is also accompanied by a small number of radial cracks. The net effect of the nose shape dependence of S_M and u_{If} is that the greatest dissipation of energy in phase I occurs for the hemi-spherically nosed indenter (24.4 J), followed by the blunt (11.3 J) and finally the conical indenter (3.6 J).

The energy dissipated during phase II for each nose shape is closely related to the mode of first fracture. For the blunt indenter, further resistance to penetration is due to bending and further crack propagation where the disc cut by the indenter remains attached to the plate. This is shown in Fig. 4, a photograph of the deformed specimen taken at the point of complete perforation of the plate. The plastic bending occurring after plug formation contributes only a little to the total energy dissipation (Fig. 3a). The mode of deformation in phase II is similar to that for the hemi-spherical nose shape, with the addition of further propagation of the radial cracks formed at the end of phase I, to form petals (Fig. 4). Again, the energy dissipated in phase II is small. For the conical indenter, further propagation of radial cracks and petal bending occurs (Fig. 4). In contrast to the other nose shapes, phase II dominates the total energy absorption for the conical indenter. The total dissipated energy for the three nose shapes is summarised in Table 2.

3.2. Impact perforation of monolithic metallic plates

A series of impact experiments were conducted on monolithic metal plates (aluminium alloy 6082-T6, $h_m = 1$ mm) using the three different projectile nose shapes. The failure modes, shown in column 1 of Fig. 5, are very similar to those observed under quasi-static loading. The most significant differences can be observed for the plates impacted by hemi-spherical and conical projectiles. For the hemi-spherical nose shape, impact loading leads to more extensive radial cracking than seen in the quasi-static case, with a larger number of distinct petals. For a conical nose shape, the number of petals also increases under dynamic loading. While typically four petals were formed under quasi-static loading, the number of petals formed under impact loading varies from four to six.

The ballistic limit and perforation energy under impact for the three nose shapes are summarised in Table 3. The perforation energy E_p is taken to be

$$E_p = \frac{1}{2} m_p V_{bl}^2 \tag{1}$$

where V_{bl} is the ballistic limit velocity and m_p the projectile mass. For all nose shapes, the perforation resistance is larger for dynamic compared to quasi-static loading. The largest increase in perforation energy occurs for the blunt projectile, followed by the hemi-spherical and conical projectiles. This difference may be attributable to inertia. The theoretical calculation of Awerbuch and Bodner (1974) shows that the effect of inertia can be larger for a blunt projectile compared to the other two nose shapes.

4. Arrangement of the layers in a bi-layer laminate

The investigation by Mohagheghian et al., in press showed that the perforation response of polymer–metal bi-layer targets impacted by a blunt indenter is sensitive to the arrangement of the

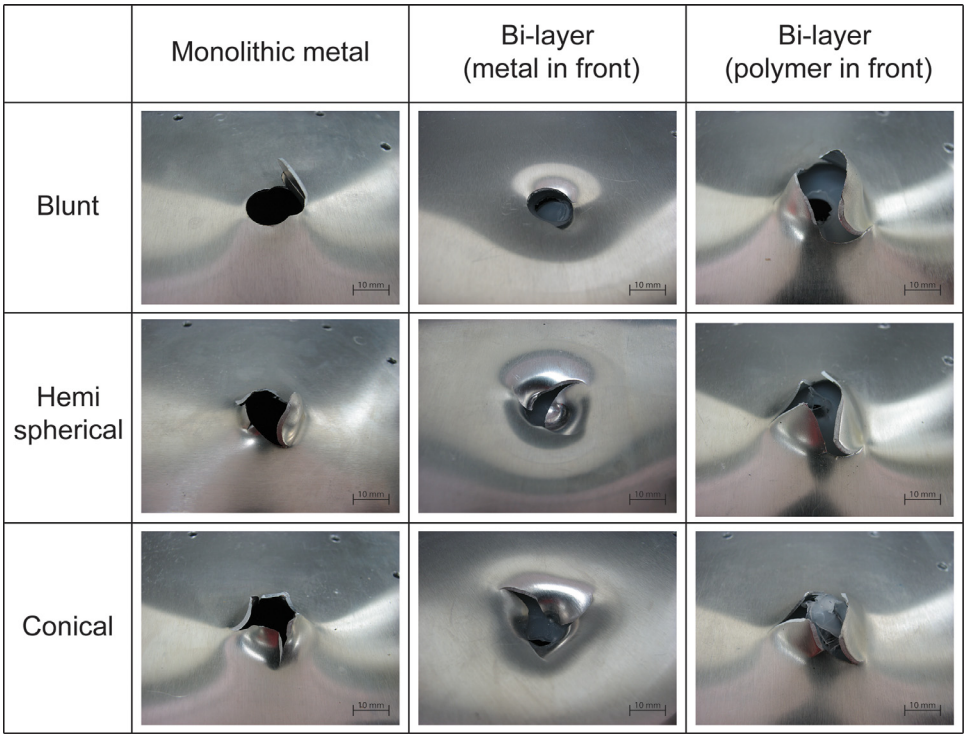

Fig. 4. Quasi-static failure modes of monolithic Al alloy ($h_m = 1$ mm) (column 1), and Al alloy-LDPE bi-layer plates ($h_m = 1$ mm and $h_p = 3$ mm) with the metal on the contacted face (column 2) and the polymer on the contacted face (column 3). For columns 1 and 3 the pictures show the back (distal) face, while for column 2 they show the front (proximal) face.

Table 2
Summary of the quasi-static perforation energies for different target configurations and indenter nose shapes.

Specimen	Nose shape	Quasi-static perforation energy (J)		
		Phase I	Phase II	Total
Monolithic metal ($h_m = 1$ mm)	Blunt	11.3	2.2	13.5
	Hemi-spherical	24.4	5.1	29.5
	Conical	3.6	14.3	17.9
Bi-layer ($h_m = 1$ mm, $h_p = 3$ mm), polymer facing indenter	Blunt	50.1	8.9	59.0
	Hemi-spherical	30.8	10.8	41.6
	Conical	10.4	24.6	35.0
Bi-layer ($h_m = 1$ mm, $h_p = 3$ mm), metal facing indenter	Blunt	12.2	16.6	28.8
	Hemi-spherical	27.8	20.3	48.1
	Conical	4.7	29.0	33.7

Table 3
Summary of the impact perforation energies for different target configurations and projectile nose shapes.

Specimen	Nose shape	Ballistic limit velocity ($m\,s^{-1}$)	Perforation energy (J)
Monolithic metal ($h_m = 1$ mm)	Blunt	57.0	32.8
	Hemi-spherical	68.5	47.4
	Conical	47.0	22.3
Bi-layer ($h_m = 1$ mm, $h_p = 3$ mm), polymer facing indenter	Blunt	94.5	90.2
	Hemi-spherical	86.0	74.7
	Conical	79.0	63
Bi-layer ($h_m = 1$ mm, $h_p = 3$ mm), metal facing indenter	Blunt	65.0	42.7
	Hemi-spherical	82.5	68.7
	Conical	79.5	63.8

layers. It was found that a significant increase in energy absorption can be achieved if the polymer, rather than the metal, is placed facing the indenter. The relationship between layer arrangement and projectile tip geometry for polymer–metal bi-layers is considered in this section.

The bi-layer test specimen consists of one metal and one polymer layer of approximately equal areal density. The metal layer is aluminium alloy 6082-T6 with thickness $h_m = 1$ mm. The polymer layer is extruded low density polyethylene (LDPE) with thickness $h_p = 3$ mm. Nominal stress–strain curves for the two materials are plotted in Fig. 2a and b, respectively. The result for the LDPE was obtained in a similar way to that described in Section 3 for the aluminium alloy. In the polymer case, the geometry of the tensile dog-bone specimens machined from the extruded plate follow ASTM-D638 (type V) (ASTM D638–10, 2010), with the gauge section having length 9.5 mm and width 3.2 mm. It can be seen from Fig. 2 that the LDPE has a much lower yield strength than the 6082-T6 at around 12 MPa, but a much higher

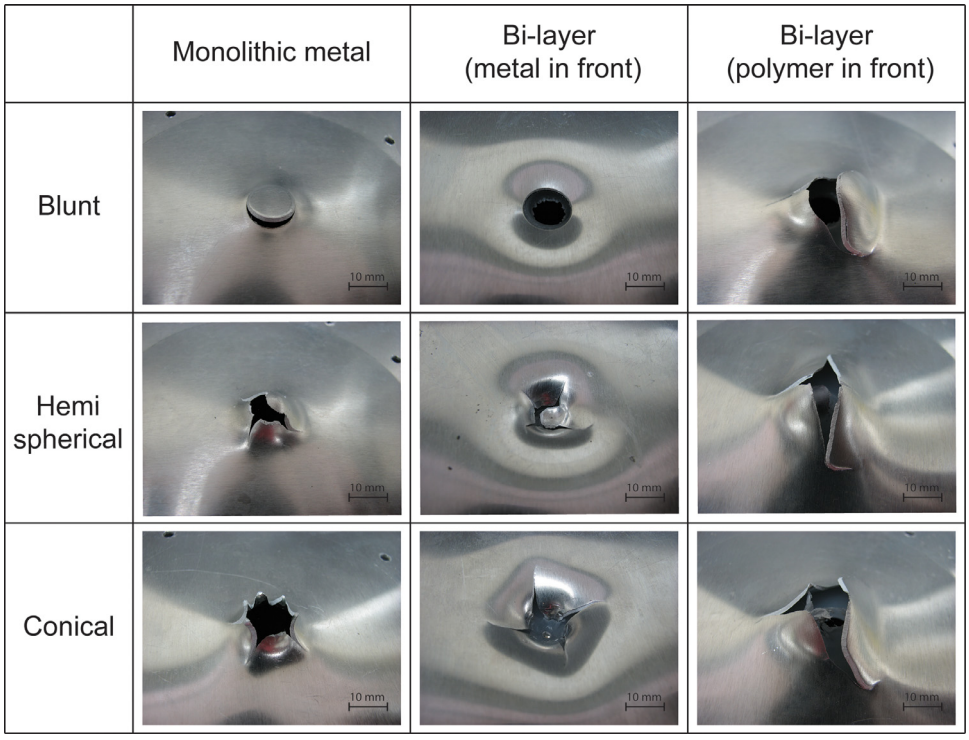

Fig. 5. Impact failure modes of monolithic Al alloy ($h_m = 1$ mm) (column 1), and Al alloy-LDPE bi-layer plates ($h_m = 1$ mm and $h_p = 3$ mm) with the metal on the impacted face (column 2) and the polymer on the impacted face (column 3). For columns 1 and 3 the pictures show the back (distal) face, while for column 2 they show the front (proximal) face.

ductility, with a nominal strain at fracture of approximately 700%. The LDPE undergoes limited strain hardening during plastic deformation. The specimen plate geometry and boundary conditions are given in Fig. 1. The two layers (polymer and metal) are clamped together in frictional contact only: no adhesive is used between the layers.

4.1. Quasi-static perforation

The quasi-static perforation results are shown in Fig. 6 for the three indenter nose shapes. In each case, four results are shown: the metal layer alone (thickness $h_m = 1$ mm, as discussed in Section 3), the polymer layer alone (thickness $h_p = 3$ mm), and the bi-layer combination ($h_m = 1$ mm and $h_p = 3$ mm). As noted above, this polymer thickness was chosen so that the metal and polymer layers have equal areal density. Other polymer/metal ratios will be discussed in Section 5. The bi-layer plate also has twice the mass of the monolithic plates, the objective here being to study the synergy between the layers when combined. A comparison between monolithic and bi-layer plates of equal mass is given in Section 4.1.3.

4.1.1. Metal layer facing the indenter

Consider first the case with the metal layer facing the indenter, shown by the dotted line in Fig. 6. As described by Mohagheghian et al., in press, the response for the blunt indenter is almost the superposition of the responses of the two layers tested in isolation. The force-deflection plot follows that of the metal layer prior to metal fracture, and then follows that of the monolithic polymer. Thus, there appears to be no synergy between the layers. This type of behaviour is also observed for the hemi-spherical indenter, with the polymer backing having no significant effect on the first onset of failure. These observations can be explained by considering the deformed shape of the plates, given in column 2 of Fig. 4. For the blunt and hemi-spherical indenters, the metal layer in the bi-layer case can be seen to fail in a very similar manner to the monolithic metal case. The polymer layer backing the metal plate appears to have no significant effect on the mode of deformation and fracture, and thus no effect on the energy dissipated in phase I. In these cases, the polymer backing has a small influence on dissipation in phase II (Fig. 6), where it resists bending of the fractured metal plate.

It should be noted, however, that no adhesive is used to bond the layers in this study. As suggested by Xue and Hutchinson (2007), a strongly adhered polymer could potentially retard the onset of necking of the metal layer (and subsequently postpone fracture) if the polymer incremental stiffness is sufficiently large. For the material combination used here, a tangent modulus greater than 173 MPa is needed for the polymer layer to be effective in that regard, based on the analysis in Xue and Hutchinson (2007). However, for the polyethylenes used, yielding occurs at a true strain of around 0.05, and the incremental stiffness subsequently drops significantly and remains low up to true strain of about 1 (Bartczak, 2005, 2010). This is the range of strains for which necking occurs in the aluminium layer. As a result, even in the presence of strong adhesion, this is not a synergistic mechanism that can be expected to occur for the material combination considered here.

The polymer backing has the greatest influence on the response of the plate to the conical indenter. Although the response is similar to that of the monolithic metal before the onset of fracture (the first load drop), the polymer backing significantly increases the energy absorption in phase II (as defined in Section 3). This can again be explained by considering the deformed shape of the plates given in Fig. 4. In contrast to the other two nose shapes, the polymer backing does alter the mode of failure of the metal layer for the conical indenter. Fewer petals develop, i.e. three instead of four that were seen in the monolithic metal case. While this does not significantly alter the energy dissipated in phase I (Fig. 6), rotation of these large petals in phase II requires stretching and tearing of the polymer layer. This leads to the

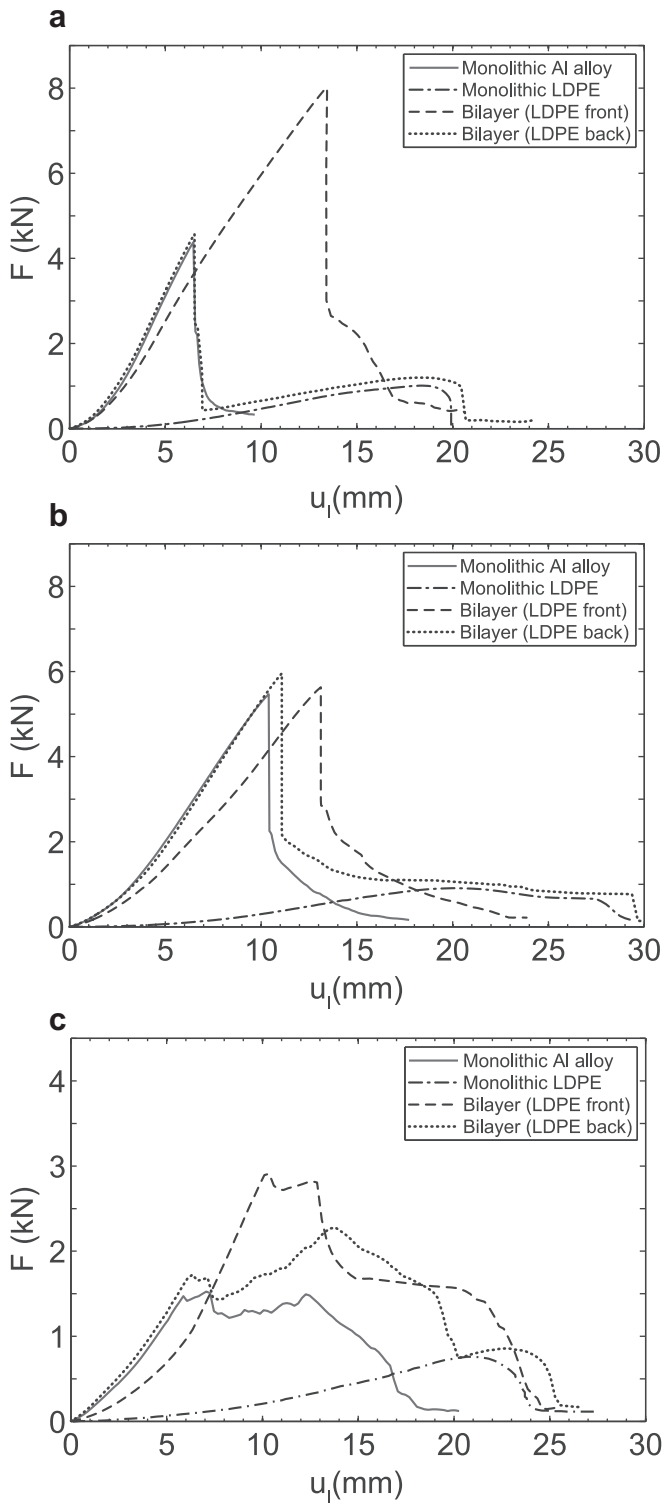

Fig. 6. Quasi-static indentation response of Al alloy-LDPE bi-layer laminates with $h_m = 1$ mm and $h_p = 3$ mm. Two orientations are shown: polymer on the contacted face (labelled 'LDPE front') and metal on the contacted face (labelled 'LDPE back'). Monolithic results are given for Al alloy ($h_m = 1$ mm) and LDPE ($h_p = 3$ mm). Indenter nose shapes are (a) blunt, (b) hemi-spherical and (c) conical.

increase in resistance to perforation after the initial drop in load, as seen in Fig. 6c.

4.1.2. Polymer layer facing the indenter

Consider next the response of the bi-layer plate with the polymer layer facing the indenter, depicted by dashed line in Fig 6. As described by Mohagheghian et al., in press, placing the polymer layer between a blunt indenter and the metal sheet causes a significant delay in the initiation of failure in the metal layer, and this in turn leads to additional plastic deformation and energy absorption in phase I (Fig. 6). A similar delay in the onset of fracture can be seen for the other indenter nose shapes as well. However, the influence of the polymer layer is not as significant as observed for the blunt indenter. These observations can again be explained by considering photographs of the fully perforated bi-layer plates (given in column 3 of Fig. 4) illustrating the failure modes under the three indenters. Mohagheghian et al., in press attributed the performance of the bi-layer plate when loaded by the blunt indenter to a change in the effective nose shape of the projectile, increasing the amount of dishing deformation and altering the mode of failure from fracture at the perimeter of the indenter (plugging) to tensile tearing at the centre of the plate. For the hemi-spherical and conical indenters, a similar increase in dishing deformation is observed (Fig. 4), indicating that the polymer is having a similar effect in these cases. The polymer layer also appears to induce a similar mode of failure in the metal layer for all three nose shapes. The absence of adhesive between the polymer and metal layers is believed to have a negligible effect on the performance in this configuration. Roland et al. (2010) observed no significant effect of adhesive for a steel–elastomer combination, when the elastomer is placed facing the projectile.

4.1.3. Synopsis of the quasi-static perforation of alternative bi-layer arrangements

The net effect of the phenomena described above is summarised in Fig. 7a: the quasi-static perforation energies of bi-layers with either metal or polymer facing the three different indenter geometries. The bi-layer results are compared with three monolithic plate configurations: $h_m = 1$ mm aluminium alloy (equal to the metal layer in the bi-layer plate), $h_p = 3$ mm LDPE (equal to the polymer layer in the bi-layer plate) and $h_m = 2$ mm aluminium alloy (which has the same weight as the bi-layer plate). The two thicknesses of monolithic metallic plate enable two separate comparisons: the bi-layer versus the bare substrate (i.e. the 'retro-fit' comparison), and the bi-layer versus monolithic metal on an equal weight basis.

For all three nose shapes, the monolithic metal plate with thickness $h_m = 2$ mm outperforms the bi-layer solution with the metal located on the contacted face. The perforation energy for this bi-layer configuration is approximately the sum of the values for the constituent layers tested separately, indicating little synergy between the layers. The thicker monolithic solution outperforms the bi-layer solution by the greatest margin for the conical projectile. These trends can be explained by the different scaling relationships between perforation energy and plate thickness for monolithic plates loaded by different tip geometries. For a hemi-spherical tip, the analysis of Simonsen and Lauridsen (2000) predicts a linear dependence of perforation energy on plate thickness h_m, assuming the plate is thin and deforms by membrane stretching. However, the analysis by Wierzbicki (1999) shows that when the perforation energy is dominated by petal bending, as is the case for the conical tip, the perforation energy scales with $h_m^{1.6}$. This greater sensitivity to plate thickness explains the benefit offered by the thicker metallic target for the conical indenter tip.

For both the conical and hemi-spherical indenter geometries, the two bi-layer configurations perform similarly. The net effect of placing the polymer on the contacted face, and hence the effective nose shape change this softer layer induces, is not large. However, for the blunt indenter the effect is significant. This was explained by Mohagheghian et al., in press, who demonstrated that increasing the tip curvature of a blunt indenter can lead to a

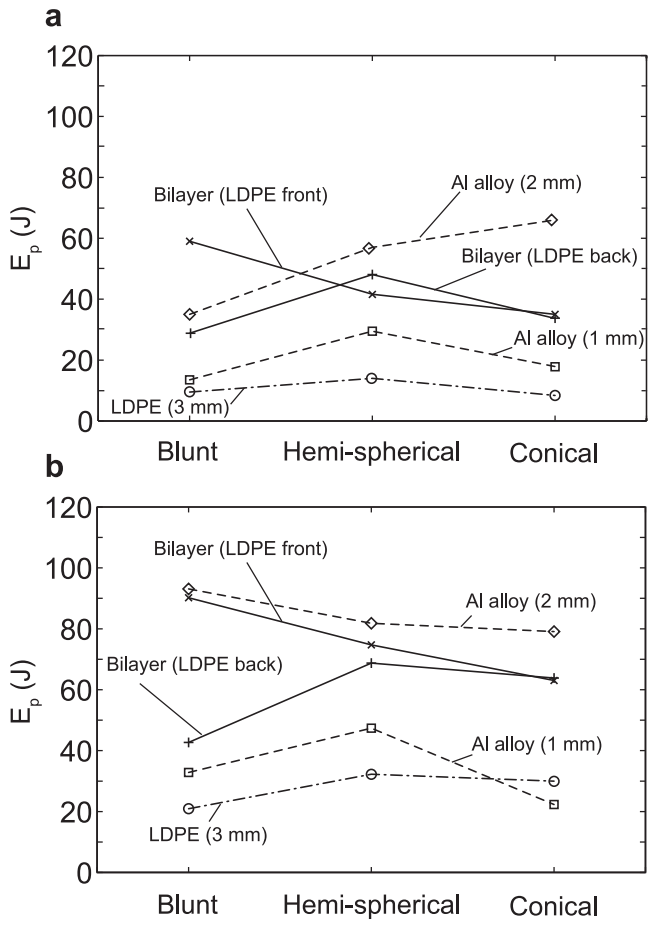

Fig. 7. Comparison of the perforation energies of monolithic and bi-layer plates subjected to (a) quasi-static loading and (b) impact loading. Bi-layers are Al alloy-LDPE, with $h_m = 1$ mm and $h_p = 3$ mm. Two orientations are shown: polymer on the contacted face (labelled 'LDPE front') and metal on the contacted face (labelled 'LDPE back'). Monolithic results are given for Al alloy ($h_m = 1$ mm and 2 mm, the latter the same weight as the bi-layer) and LDPE ($h_p = 3$ mm).

substantial increase in perforation resistance. Consequently, for this tip geometry only, the bi-layer configuration with the polymer on the contacted face can outperform an equal weight monolithic metal solution.

4.2. Impact perforation

Next, the influence of dynamic effects on these conclusions is examined. A comparison of the impact perforation modes for bi-layer plates with polymer layer thickness $h_p = 3$ mm (LDPE) and metal layer thickness $h_m = 1$ mm (6082-T6) is shown in Fig. 5. Two cases are shown, with either the metal or the polymer on the impacted face. Comparing the deformed shapes with the quasi-static equivalents in Fig. 4, it can be seen that the influence of the polymer layer—in either orientation—is similar for both quasi-static and dynamic loading. For these lightweight targets, dynamic effects do not appear to substantially alter the mode of failure.

A key phenomenon observed quasi-statically was the effective nose shape change induced by placing the polymer on the impacted face. To confirm the presence of this effect during impact loading, profilometry was used to measure the permanent deformation of monolithic and bi-layer targets impacted at a velocity just sufficient to induce fracture in the metal layer (Fig. 8). The polymer layer (which has sprung back elastically in Fig. 8, losing contact with the metal backing) results in more extensive plastic deformation in the metal layer, and a convergence in the nature and location of fracture between the various nose shapes. This is consistent with the quasi-static results.

The impact perforation energies for the two bi-layer and three monolithic cases are summarised in Fig. 7b, for comparison with the quasi-static equivalents in Fig. 7a. Although the perforation energies are higher, due to inertia and material strain rate sensitivity (the latter being particularly important for the polymer layer (Mohagheghian et al., 2015), aluminium alloy 6082 T6 having very low strain rate sensitivity (Oosterkamp et al., 2000; Chen et al., 2009)), the trends in performance largely match those seen under quasi-static loading. This is consistent with the similarity in the modes of deformation and failure. However there is one notable exception. For the blunt projectile, the relative performances of the bi-layer case (polymer facing the projectile) and the thicker monolithic plate are reversed under dynamic loading. The large dynamic elevation in perforation resistance of the thicker metallic target in this case is key, and is likely to be attributable to the contribution of inertia to the plugging failure mode. As a result, the bi-layer configurations underperform the monolithic metal solution of equal weight for all three tip geometries, for this particular polymer type and layer thickness combination.

5. Polymer layer thickness

From the results of Section 4 it is concluded that the most effective location of the polymer layer in a bi-layer target is on the impacted face, where its predominant contribution to perforation energy is to enhance the plastic deformation of the metal layer by altering the effective projectile tip geometry. This is the case, to a greater or lesser extent, for all three indenter nose shapes. In the following, the influence of the polymer layer thickness on this mechanism is investigated for each tip geometry. To achieve this, a series of quasi-static and impact perforation tests were conducted on plates with a fixed metal layer thickness ($h_m = 1$ mm, aluminium alloy 6082-T6) and various LDPE layer thicknesses ($h_p = 1.6$, 3.0, 4.5 and 5.9 mm, i.e. up to about six times the metal layer thickness). In all cases, the polymer is placed facing the indenter. This range of polymer layer thicknesses means that we cover a range of polymer layer/metal layer areal density ratios of around 0.5–2 (thus spanning the case presented in Section 4, where the two layers had equal areal density). We opt to achieve this with a fixed metal layer thickness in order to systematically assess the influence of the polymer thickness on the mode of failure. Note that the total mass of the bi-layer plates will therefore increase with the polymer layer thickness. A comparison of monolithic and bi-layer performance on an *equal mass* basis is described subsequently, in Section 5.2.

5.1. Quasi-static perforation

The indenter force–displacement results for bi-layers with different polymer thicknesses are shown in Fig. 9 for the three indenter nose shapes. The variation in total perforation energy (defined as the area under the indenter force–displacement curve) with polymer layer thickness is plotted in Fig. 10. These results are further decomposed into the work done before and after first fracture of the metal layer (phases I and II, respectively).

5.1.1. Influence of the polymer layer thickness on the failure mode

For a blunt indenter, as described in Mohagheghian et al., in press, a thin layer of polymer can alter the effective indenter nose shape sufficiently to significantly delay the onset of failure. Further increases in polymer layer thickness have a diminishing effect. This is reflected in the force–displacement curves (Fig. 9a). This diminishing effect can be better understood by considering the decomposition of the perforation energy into the phase I and phase II

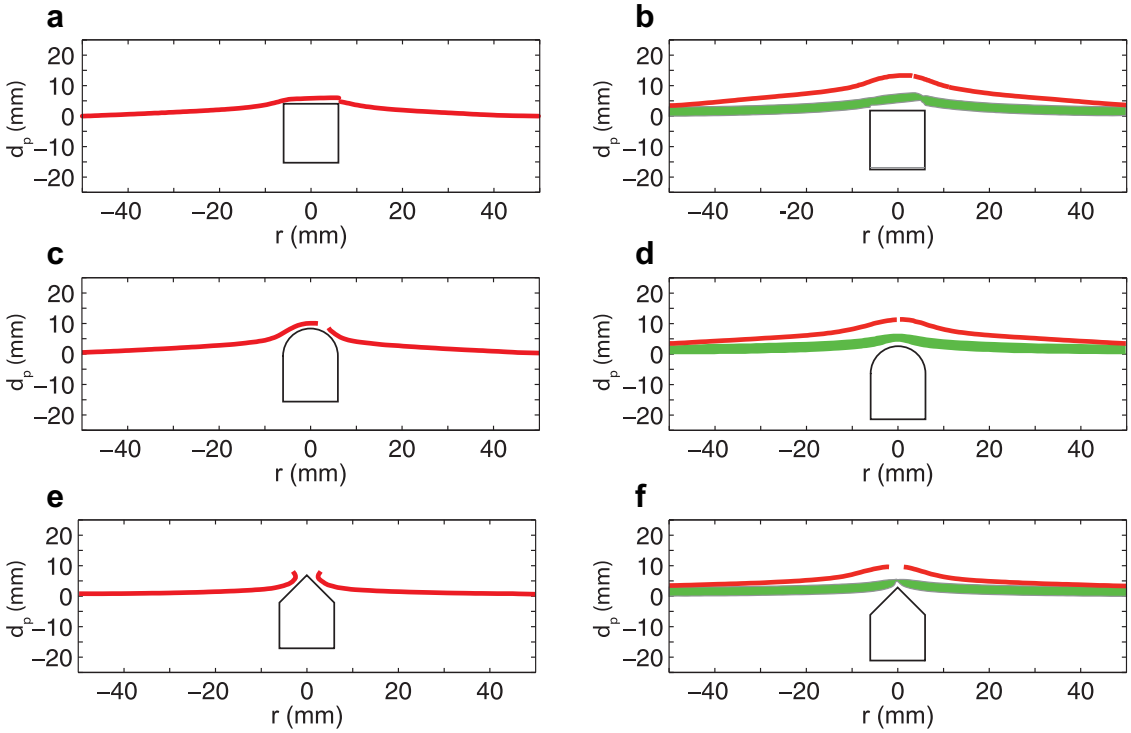

Fig. 8. Profilometry of monolithic Al alloy targets ($h_m = 1$ mm) and Al alloy-LDPE bi-layers ($h_m = 1$ mm, $h_p = 3$ mm) impacted on the polymer face, measured at the onset of fracture in the metal layer. The plates are impacted by (a and b) blunt, (c and d) hemi-spherical and (e and f) conical projectiles.

contributions, as defined above, and comparing cases with increasing polymer thickness. The deformed plates at the end of phases I and II are shown in Fig. 11. The transition, with increasing polymer thickness, from failure at the projectile perimeter (plugging) to bulging and tensile failure at the centre of the plate accounts for the large initial rise in phase I dissipation Mohagheghian et al., in press. However, after this transition has completed, the phase I energy (predominantly due to dishing of the metal layer) plateaus. Further increasing the polymer thickness leads to a smaller additional rise in perforation energy, mainly as a result of the increase in the energy absorbed in phase II (Fig. 10). This failure mode transition has been analysed further in Mohagheghian et al., in press.

In contrast, for the conical and hemi-spherical indenters, a thin layer of polymer does not significantly affect the onset of fracture or total energy absorption (Figs. 9 and 10). Rather than reaching a plateau, as in the blunt case, the total perforation energy continues to rise with increasing polymer thickness. As shown in Fig. 10, this is largely attributable to a rising trend in phase I energy absorption in these cases. This can be explained by considering the deformed plates shown in Fig. 11. For the conical indenter, when the polymer layer is thin, no significant increase in dishing deformation is observed, as the indenter tip easily perforates the polymer layer and initiates petalling in the metal substrate. As the polymer thicknesses is increased, this failure mechanism is delayed to larger indenter displacements, and more extensive dishing deformation can occur in the metal layer as a result: compare the cases with $h_p = 1.6$ mm and 5.9 mm in Fig. 11, at the end of phase I. For polymer layer thicknesses above 3 mm (i.e. $h_p/h_m > 3$), energy absorption in phase I begins to rise more steeply (Fig. 10c). This thickness is equal to the height of the conical tip of the indenter. For the hemi-spherical indenter, the presence of even a thin polymer layer alters the contact conditions between the indenter and metal plate and moves the location of fracture to the centre of the plate (Fig. 11). However, this does not significantly increase the perforation energy. Further increasing the polymer layer thickness is required in order to alter the effective tip geometry, and consequently to increase the level of dishing deformation achieved when the metal layer first fractures.

5.1.2. Failure mode convergence

Finally, it is noted from Fig. 10 that when the ratio of the polymer thickness to the indenter radius approaches $h_p/R_I = 1$ (i.e. $h_p/h_m \approx 6$), the total perforation energies for the three indenter nose shapes converge. The performance of the bi-layer plates becomes insensitive to the indenter nose shape. As shown in Fig. 11, at these larger polymer layer thicknesses, the deformed shapes and modes of failure of the plates are very similar.

5.2. Impact perforation

For impact loading of bi-layer plates, the same transition in failure mode is observed with increasing polymer thickness. Similar to the quasi-static case (Fig. 11), increasing the polymer layer thickness reduces the number of petals and increases their size. The variation in perforation energy with polymer layer thickness is summarised in Fig. 12. For all three nose shapes, the trends in perforation energy are similar under both quasi-static and dynamic loading. In both cases, the responses of the three nose shapes converge as the polymer thickness approaches $h_p/R_I = 1$ ($h_p/h_m \approx 6$). However, the perforation energies are consistently higher in the impact case, with the difference increasing with polymer thickness. As noted above, this can be attributed to the contributions of inertia and material strain rate sensitivity. The former will depend on the mode of deformation and failure and, hence, the polymer layer thickness. The latter is also dependent on the thickness of the polymer layer, as the yield strength of LDPE is more sensitive (Mohagheghian et al., 2015; Walley and Field, 1994) to strain rate than that of aluminium alloy 6082 T6 (Oosterkamp et al., 2000; Chen et al., 2009).

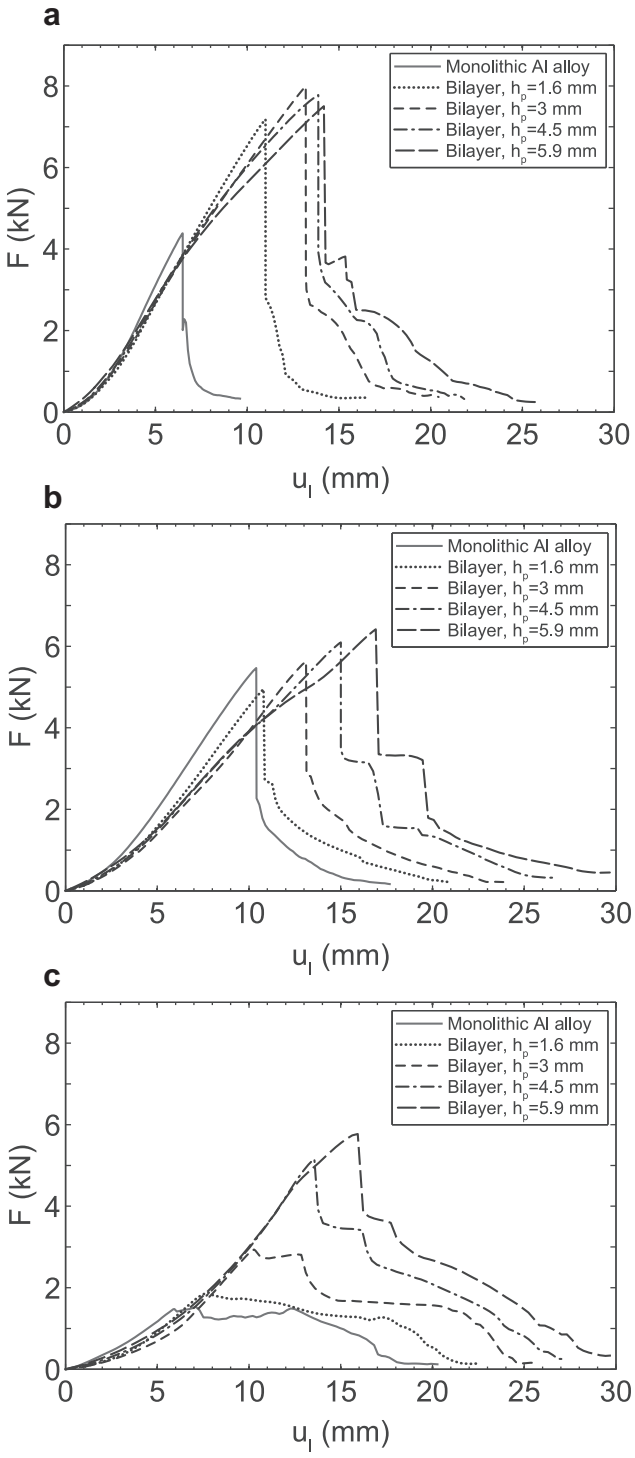

Fig. 9. Quasi-static indentation response of Al alloy-LDPE bi-layer laminates with $h_m = 1$ mm and different polymer thicknesses, h_p. The polymer is located on the contacted face. Monolithic results are given for Al alloy ($h_m = 1$ mm). Indenter nose shapes are (a) blunt, (b) hemi-spherical and (c) conical.

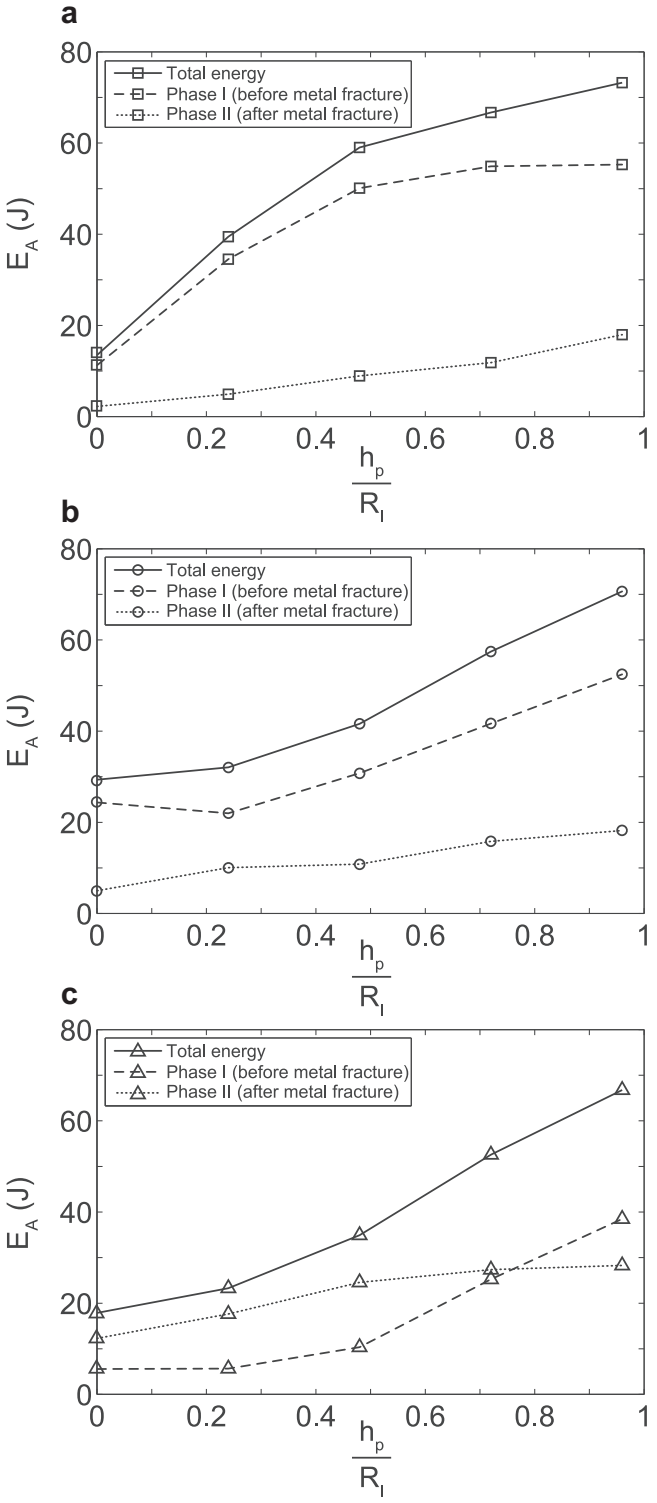

Fig. 10. Decomposition of the total absorbed energy (E_A) into the contributions before (phase I) and after (phase II) metal fracture, for the quasi-static indentation of bi-layer plates. Al alloy-LDPE bi-layer plates with $h_m = 1$ mm and $0 \le h_p \le 5.9$ mm, loaded on the polymer face by (a) blunt, (b) hemi-spherical and (c) conical indenters.

5.2.1. Equal mass performance comparison

The bi-layer results discussed here were obtained for plates with a fixed metallic substrate thickness ($h_m = 1$ mm), and therefore increasing the polymer layer thickness also increases the plate mass. In order to assess the competitiveness of the bi-layer solutions with monolithic targets on an equal mass basis, impact perforation experiments were performed on monolithic plates of LDPE and aluminium alloy 6082-T6 of increasing thickness, spanning the same range of areal density as the bi-layer targets. These results are plotted in Fig. 13 along with the bi-layer results for each projectile nose shape.

For the blunt projectile, Fig. 13a, the best performance for a bi-layer plate compared to the equivalent mass monolithic metal

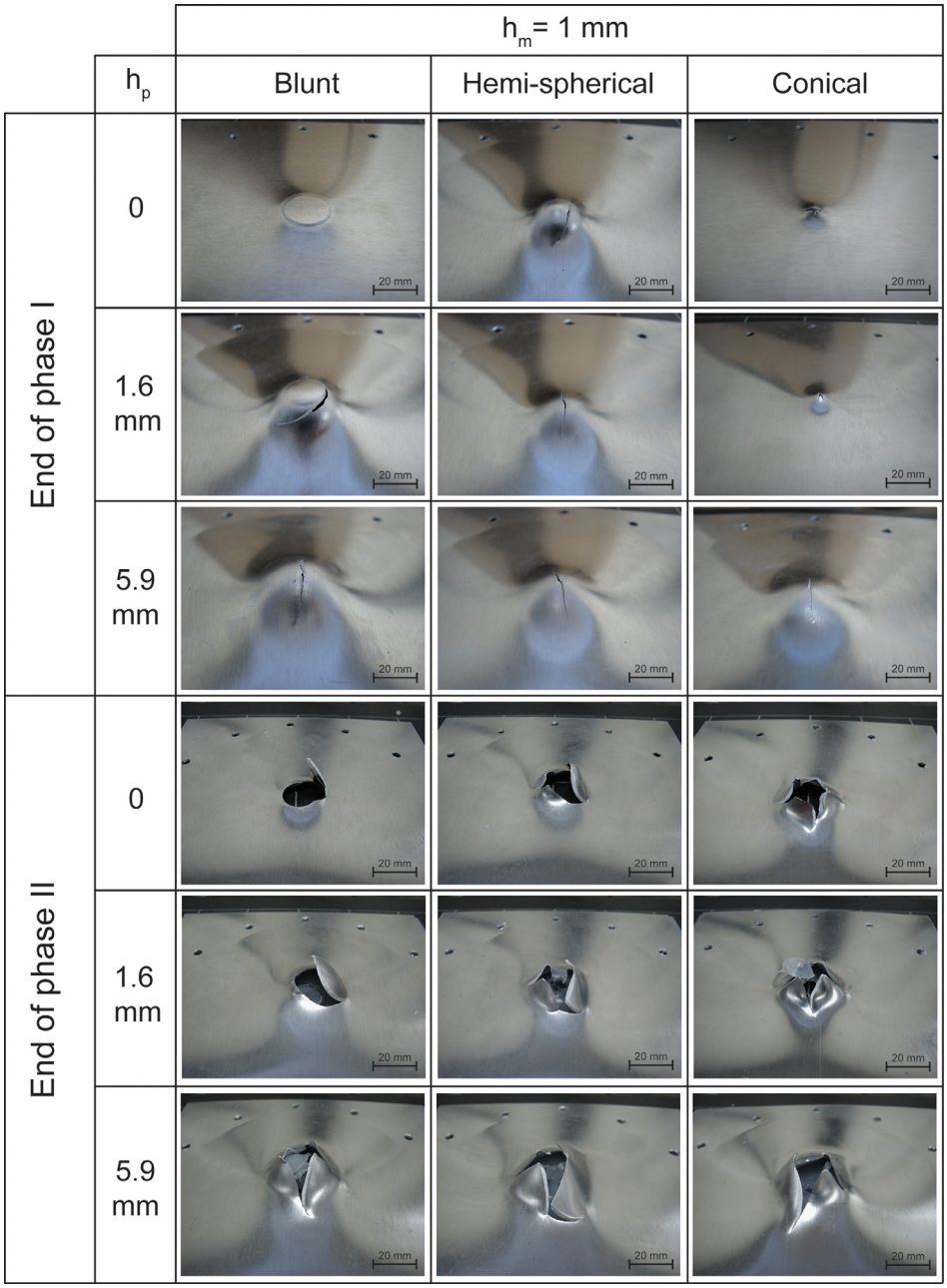

Fig. 11. Quasi-static failure modes of monolithic Al alloy ($h_m = 1$ mm) and Al alloy-LDPE bi-layer plates ($h_m = 1$ mm, $h_p = 1.6$ and 5.9 mm) with the polymer on the contacted face. The pictures show the distal face, at the end of phase I and phase II.

occurs for the configuration with an area density of 4 kg m^{-2}, which corresponds to the case $h_m = 1$ mm, $h_p = 1.6$ mm (i.e. $h_p/h_m = 1.6$). In this case, the bi-layer outperforms the monolithic target of the same weight. As described in Mohagheghian et al., in press, this configuration also corresponds to a peak in perforation energy per unit mass of plate in the bi-layer case, and coincides with both a maximum in dishing deformation and the transition point from plugging to tensile failure in the metal layer. This optimum has also been reported by Corran et al. (1983) for monolithic metallic targets impacted by projectiles with different tip radii.

Fig. 13b shows the same comparison for the hemi-spherical projectile. For this nose shape, the performance of monolithic metal, monolithic polymer and bi-layer solutions are more similar across the range of target masses. However, for plate masses in excess of 4 kg m^{-2}, the bi-layer underperforms both monolithic solutions. The conical projectile results are given in Fig. 13c. Again, the bi-layer solution underperforms that of both monolithic targets.

5.2.2. Analysis of bi-layer performance

The under-performance of bi-layer solutions for hemi-spherical and conical projectiles can be explained with reference to existing analytical solutions for the perforation energies of monolithic plates. For a bi-layer plate with metal thickness h_m and polymer thickness h_p, the mass per unit area m is given by

$$m = \rho_m h_m + \rho_p h_p, \tag{2}$$

where ρ_m and ρ_p are the densities of the metal and polymer layers, respectively. Introduce the following non-dimensional quantities: plate mass $\bar{m} = m/(\rho_m R)$, metal thickness $\bar{h}_m = h_m/R$, indenter radius $\bar{R}_I = R_I/R$ and density ratio $\overline{\rho} = \rho_m/\rho_p$. In the

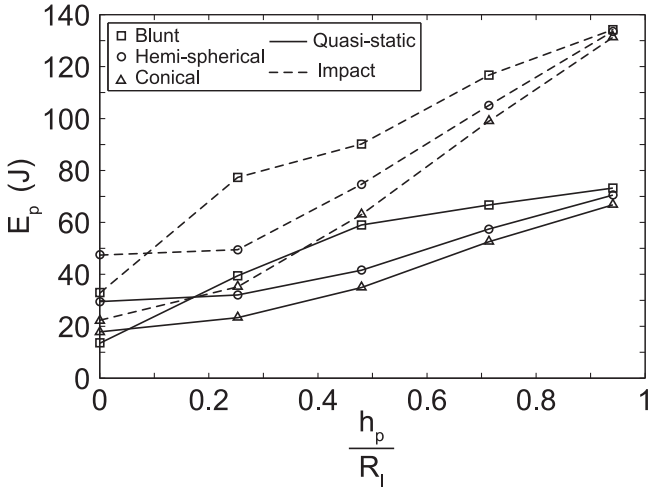

Fig. 12. Variation in perforation energy (E_p) with polymer layer thicknesses (h_p/R_I) for Al alloy-LDPE bi-layer plates loaded on the polymer face. Quasi-static and impact results are shown, for three nose shapes.

following, assume the plate mass per unit area m is varied by adjusting h_p, keeping h_m fixed, as in the experiments. Therefore $\bar{m}$ is treated as a free variable, with all other non-dimensional parameters held constant. In the current study, these constants have the values $\bar{h}_m = 0.02$, $\bar{R}_I = 0.125$ and $\bar{\rho} = 2.9$.

First consider the case of a bi-layer plate loaded by a hemi-spherical indenter in contact with the polymer face. Assuming that, during deformation, the polymer layer conforms to the indenter tip, its effective radius will be increased to $R_{I(e)}$, given by:

$$R_{I(e)} = R_I + h_p. \tag{3}$$

Here, R_I is the original indenter radius. Note that (3) neglects any thinning of the polymer layer, and thus can be considered an upper bound for the effective radius. Using the Simonsen and Lauridsen analysis (Simonsen and Lauridsen, 2000) for the deformation of a thin circular plate by a hemi-spherical indenter, with the indenter radius equal to the effective radius $R_{I(e)}$, the perforation energy of the bi-layer $E_{p(b)}$ is given by:

$$\frac{E_{p(b)}}{\sigma_0 \pi R^3} = \bar{h}_m\left(\bar{R}_I + \bar{m}\bar{\rho} - \bar{h}_m\bar{\rho}\right) \times \left\{0.318\left(\bar{R}_I + \bar{m}\bar{\rho} - \bar{h}_m\bar{\rho}\right)^{0.6} + 0.067(n - 0.2)\right\}. \tag{4}$$

Here, σ_0 and n are material parameters, defining a power law relationship between true stress and logarithmic strain for the metallic layer: $\sigma = \sigma_0\varepsilon^n$. σ_0 and n are equal to 520 MPa and 0.13 for aluminium alloy AA 6082 T6. For a comparable monolithic metal target, the indenter radius is now simply R_I, but the thickness of the metal plate is increased, in order to match the weight of the bi-layer. Thus, substituting these parameters into the Simonsen and Lauridsen analysis (Simonsen and Lauridsen, 2000), it predicts a perforation energy $E_{p(m)}$ given by:

$$\frac{E_{p(m)}}{\sigma_0 \pi R^3} = \bar{m}\bar{R}_I\left\{0.318\left(\bar{R}_I\right)^{0.6} + 0.067(n - 0.2)\right\}. \tag{5}$$

This solution to the Simonsen and Lauridsen model is valid for the range $2 < R/R_I < 10$ and $0.1 < n < 0.3$. In our case, $R/R_I = 8$ and $n = 0.13$, which lies within this range. Although the model was obtained from a quasi-static analysis, we have verified that the equation predicts the correct trends for our dynamic case. In the current investigation, the lightweight plates tested have $\bar{m} \approx 0.02 - 0.06$. Comparison of (4) and (5), after evaluating the coefficients, shows that $E_{p(m)} > E_{p(b)}$ across the full range of $\bar{m}$ considered. Hence, increasing the effective indenter radius (through a soft polymer facing) is predicted to be a less effective dissipation mechanism than increasing the metallic plate thickness, on an equal mass basis. This is consistent with the experimental observations. Note that if thinning of the polymer layer during indentation was accounted for in this analysis, the predicted performance benefit of the monolithic solution would increase further.

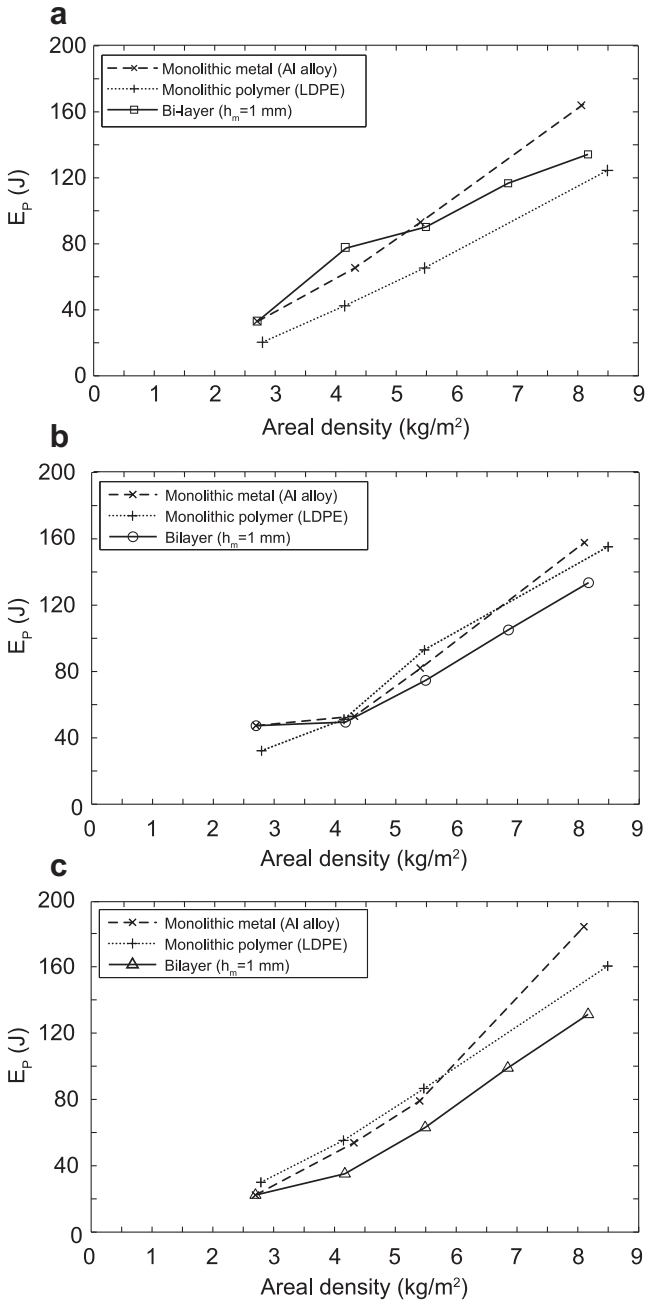

Fig. 13. Variation in the impact perforation energy (E_p) with increasing plate mass per unit area for Al alloy-LDPE bi-layer targets, with fixed metal thickness ($h_m = 1$ mm) and increasing polymer thickness ($0 \le h_p \le 5.9$ mm). The bi-layer is impacted on the polymer face, by (a) blunt, (b) hemi-spherical and (c) conical projectiles. Monolithic metal and polymer targets are shown over the same mass range for each nose shape. Note that the bi-layer curve starts with $h_p = 0$, which coincides with the monolithic metal result for $h_m = 1$ mm.

A similar approach can be applied to the conical projectile. For bi-layer cases where the perforation energy is still predominantly due to petal bending, the analysis of Wierzbicki (1999) can be used. Again, for the bi-layer targets, assume that only the

metal layer contributes to the plastic work done (in petal bending), but the polymer layer increases the effective radius of the projectile, as given by (3). A larger projectile radius requires additional petal bending to allow the projectile to pass through and complete perforation. Substituting these parameters into the model of Wierzbicki (1999) gives the perforation energy of the bi-layer $E_{p(b)}$ to be:

$$\frac{E_{p(b)}}{\sigma_y \pi R^3} = 2.83 \bar{h}_m^{1.6} \left(\bar{R}_l + \bar{m}\bar{\rho} - \bar{h}_m \bar{\rho} \right)^{1.4} . \quad (6)$$

Here, σ_y is the yield strength of the metal, assuming rigid-perfectly plastic behaviour (Wierzbicki, 1999). For a monolithic metal plate of equal mass to the bi-layer, the indenter radius is now R_l, but the thickness of the metal (and hence the bending resistance of the petals) is larger. Using the Wierzbicki (1999) analysis, the perforation energy of the equivalent mass monolithic plate $E_{p(m)}$ is therefore:

$$\frac{E_{p(m)}}{\sigma_y \pi R^3} = 2.83 \bar{m}^{1.6} \bar{R}_l^{1.4} . \quad (7)$$

Comparison of (6) and (7) again predicts that $E_{p(m)} > E_{p(b)}$, across the range $\bar{m} \approx 0.02 - 0.06$ considered in the experiments. The difference between the bi-layer and monolithic solutions is also larger in this case compared to the hemi-spherical tip, which is also consistent with the experimental observations. For petalling failure therefore, the analysis shows that it is more effective to increase the thickness of the metal layer, than to increase the radius of the indenter via a polymer facing, on an equal mass basis.

6. Influence of the polymer layer mechanical properties

Mohagheghian et al. (2015) showed that the key mechanical characteristics influencing the impact perforation resistance of ductile polymers is sensitive to the projectile nose shape. For blunt and hemi-spherical projectiles, it was found that a high degree of strain hardening was key to increasing perforation resistance. For a conical projectile, a higher polymer yield strength was of most benefit. In this section, the influence of the polymer properties on the performance of polymer–metal bi-layer targets is considered for the three different projectile nose shapes. In particular, it is determined whether the choice of polymer can increase the competitiveness of a bi-layer solution versus an equal mass monolithic metal target.

One configuration of bi-layer plate is considered: polymer thickness $h_p = 3$ mm and metal thickness $h_m = 1$ mm, with the polymer placed facing the indenter. Aluminium alloy 6082-T6 is used for the metal layer. Three different polyethylenes are considered for the polymer layer: low density (LDPE), high density (HDPE) and ultra-high molecular weight (UHMWPE). These polymers have distinct microstructures and mechanical properties, yet have densities that vary only over a small range: 930 kg m^{-3} for LDPE, 960 kg m^{-3} for HDPE and 940 kg m^{-3} for UHMWPE. Therefore, the weight of the target remains essentially insensitive to the choice of polymer, to ensure a fair comparison. The quasi-static uniaxial tensile responses of the three polymers are plotted in Fig. 2b. The techniques used to obtain these curves was as described for the LDPE specimens in Section 4. The HDPE has the highest yield strength, but also undergoes a large drop in stress after yielding due to neck formation. The quasi-static tensile ductility of HDPE is considerably larger than LDPE. In contrast to the other polymers, UHMWPE has significant strain hardening with no sign of necking during the test.

6.1. Quasi-static perforation

The indenter force–displacement plots are given in Fig. 14 for the three nose shapes. In all three cases, despite contrasting mechanical properties, the responses are insensitive to the polymer type. However three effects are noted: (i) The higher yield strength polymers slightly increase the slope of the curve during phase I, when indentation and plastic deformation of the polymer occurs. This is most significant for the HDPE, which has the highest yield strength. (ii) A higher degree of strain hardening in the polymer layer (most notable for UHMWPE) leads to a delay in the onset in fracture in the metal layer for the blunt and hemi-spherical nose

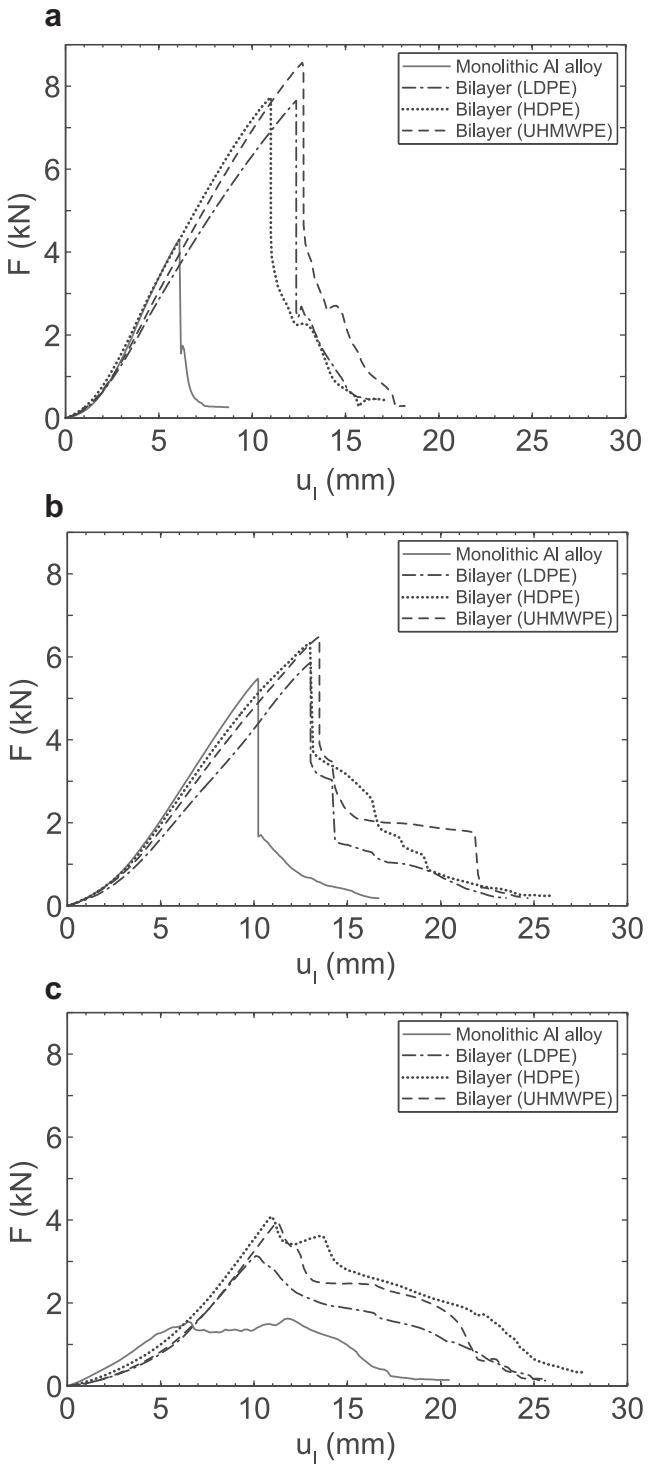

Fig. 14. Quasi-static indentation response of bi-layer laminates with $h_m = 1$ mm and $h_p = 3$ mm, loaded on the polymer face, with three different polymer types: LDPE, HDPE and UHMWPE. Monolithic results are given for Al alloy ($h_m = 1$ mm). Indenter nose shapes are (a) blunt, (b) hemi-spherical and (c) conical.

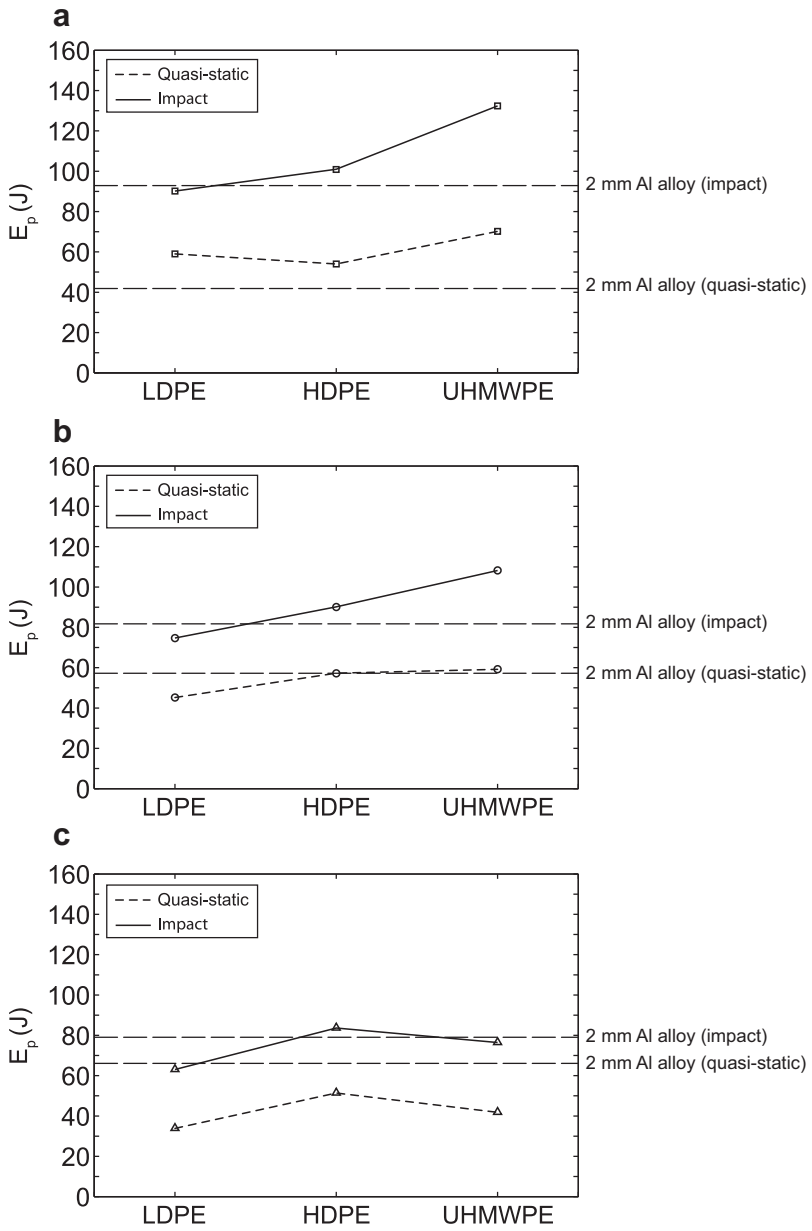

Fig. 15. Comparison of the perforation energy (E_p) for bi-layer plates ($h_m = 1$ mm and $h_p = 3$ mm) with three different polymer types (LDPE, HDPE and UHMWPE). The polymer layers are located on the impacted face. Results are also shown for monolithic metallic plates of the same mass ($h_m = 2$ mm). Quasi-static and impact results are given for (a) blunt, (b) hemi-spherical and (c) conical nose shapes.

shapes. As observed by Mohagheghian et al. (2015) for monolithic UHMWPE targets, high strain hardening delays deformation localisation and failure in the polymer layer for these nose shapes. In the bi-layer case, delaying deformation localisation in the polymer layer in turn delays the onset of fracture in the metal layer. Conversely, it was shown by Mohagheghian et al. (2015) that HDPE is more susceptible to shear localisation than the other two polymers. This is reflected in the earlier onset of metal fracture in the bi-layer with HDPE, when loaded by a blunt indenter. (iii) A higher polymer yield strength delays the onset of fracture in the metal layer for the conical projectile. This is again consistent with the observations of Mohagheghian et al. (2015): high yield strength delays the perforation of a polymer layer loaded by a conical tip geometry, and hence the failure of the metal layer is also delayed. The net effect of (i)–(iii) on the perforation energy is summarised in Fig. 15.

6.2. Impact perforation

The study by Mohagheghian et al. (2015) on the strain rate sensitivity of these three polyethylenes showed that impact loading is likely to amplify the effects (i)–(iii) described in the previous section. The yield strengths of the polymers increase with strain rate, as does the high degree of strain hardening of the UHMWPE, and the susceptibility of HDPE to shear localisation. As shown in Fig. 15, the net effect of this is to improve the performance of the bi-layer solutions compared to the equivalent mass monolithic metal target in most cases. The increased strain hardening of UHMWPE under dynamic loading provides a particular benefit in the case of blunt and hemi-spherical projectiles, delaying deformation localisation and failure of the polymer layer. For the conical projectile, the relative performance of the three polymer types is similar for both impact and quasi-static loading. As noted above,

the polymer yield strength is a key parameter for this nose shape, and the strain rate sensitivity of the yield strength is similar for all three polymers (Mohagheghian et al., 2015).

7. Conclusions

The performance of polyethylene/aluminium alloy bi-layer plates under quasi-static and impact loading conditions was studied for three contrasting nose shapes. The effect of the position, thickness and material properties of the polyethylene layer has been investigated. For the range of target configurations considered in this study the following conclusions can be made:

- For bi-layer plates with metal and polymer layers of equal mass, the sensitivity of the perforation resistance to the orientation of the layers is strongly dependent on the projectile nose shape. The effect is most pronounced for a blunt projectile, for which positioning the polymer layer facing the projectile delivers significantly better perforation resistance. In this case, the polymer alters the effective nose shape of the projectile and consequently delays the onset of failure in the metal layer as well as changing the failure mode.
- For this bi-layer configuration, when the polymer layer is oriented such that the metal faces the indenter, the performance of the bi-layer strongly depends on the mode of failure in the metal plate, which in turn depends on the projectile nose shape. A polymer backing layer provides more resistance to petal bending, which increases the resistance to perforation for a conical projectile. For blunt and hemi-spherical projectiles, where the contribution from petal bending is less, the polymer backing layer is less effective.
- The sensitivity of the perforation resistance to the polymer/metal thickness ratio (with the polymer on the impacted face) is also projectile nose-shape dependent. For the blunt projectile, a thin layer of polymer (small h_p/R_l) facing the projectile is sufficient to induce a failure mode transition and increase energy absorption. However, a thicker layer is needed to see a significant rise in perforation resistance for both conical and hemi-spherical projectiles. In the conical case, this is because the sharp tip can perforate thin polymer layers and initiate fracture in the metal without any significant change in the effective nose shape. For the hemi-spherical case, it is because the thin polymer layer has a less significant effect on the (already rounded) tip geometry than in the sharp-edged blunt case.
- For thicker polymer layers placed on the impacted face, the difference in the perforation energy between the different projectile nose shapes diminishes. For polymer layers with $h_p/R_l \approx 1$, the plate response is almost independent of the original nose shape geometry. This loss of nose shape sensitivity can be attributed to a convergence in the effective nose shape change induced by the deforming polymer layer, evident in a convergence in the mode of deformation and failure of the metal layer.
- For bi-layer plates with metal and polymer layers of equal mass, and the polymer placed on the loaded face, the type of polyethylene used has little influence on the quasi-static perforation energy. However, the differences become more pronounced under dynamic loading conditions. Dynamic loading results in an elevation in perforation energy in all cases. However, the increase is largest for UHMWPE loaded by blunt or hemi-spherical projectiles. This is attributed to the strain rate dependence of the strain hardening, a distinctive characteristic of this polymer, which delays the onset of localisation in the polymer layer.
- The perforation resistance of a thin metallic plate can be significantly improved by adding a soft polymer layer. This could find application in structural retro-fit. On an equal weight basis, the polymer metal bi-layer can outperform monolithic metal, but only for particular choices of both the polymer type and the polymer to metal thickness ratio.

Acknowledgements

The authors are grateful for joint financial support from the Engineering and Physical Sciences Research Council (EPSRC) and the Defence Science and Technology Laboratory (DSTL) through project EP/G042756/1 (Polymer Nanocomposites for Light Armour Applications). We acknowledge the EPSRC instrument loan pool for the use of the high speed camera (Vision Research Phantom V710).

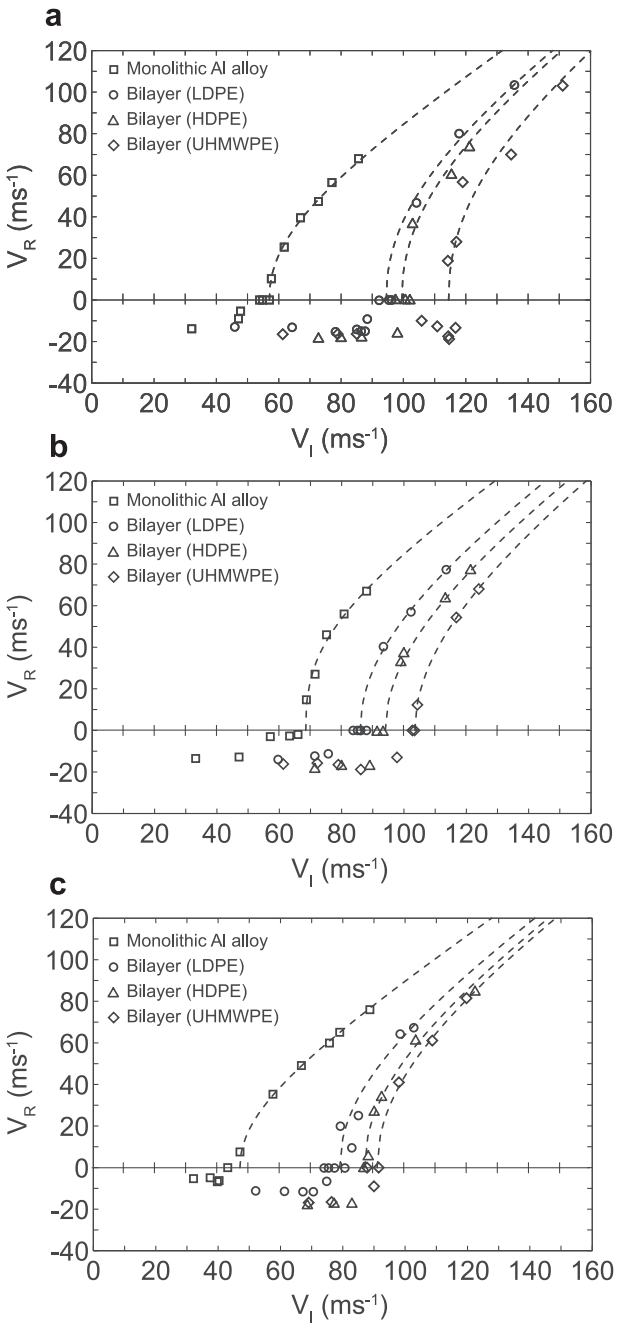

Fig. A1. Residual velocity (V_R) versus initial impact velocity (V_I) for monolithic aluminium alloy ($h_m = 1$ mm and 2 mm) and bi-layers with LDPE, HDPE and UHMWPE ($h_m = 1$ mm and $h_p = 3$ mm) for (a) blunt, (b) hemi-spherical and (c) conical projectiles.

Table A1
Ballistic limit and fitting parameters for the Lambert and Jonas relationship (Lambert and Jonas, 1976) for monolithic aluminium alloy ($h_m = 1$ mm and 2 mm) and bi-layers with LDPE, HDPE and UHMWPE ($h_m = 1$ mm and $h_p = 3$ mm) for (a) blunt, (b) hemi-spherical and (c) conical projectiles.

	Blunt			Hemi-spherical			Conical		
	V_{bl} (m s^{-1})	a	p	V_{bl} (m s^{-1})	a	p	V_{bl} (m s^{-1})	a	p
Monolithic Al alloy ($h_m = 1$ mm)	57	1	2.2	68.5	1	2.7	47	1	2.1
Monolithic Al alloy ($h_m = 2$ mm)	96	1	2.2	90	1	2.1	88.5	1	2
Bilayer (LDPE)	94.5	1	2.2	86	1	2.1	79	1	2.1
Bilayer (HDPE)	99.5	1	2.2	94	1	2	91	1	2.1
Bilayer (UHMWPE)	114.5	1	2.2	103.5	1	2	87	1	2

Appendix

In order to measure the ballistic limit, and hence the perforation energy under dynamic loading (Eq. (1)), a series of impact experiments was performed as described in Section 2.2. Fig. A1, shows the residual velocity (V_R) against the projectile initial velocity (V_I) for five different configurations including the monolithic aluminium alloy plate (1 mm and 2 mm thicknesses) and bi-layers with $h_m = 1$ mm and $h_p = 3$ mm, for three different polymer types: LDPE, HDPE and UHMWPE. The polymer is located facing the projectile in all bi-layer cases. A positive residual velocity (V_R) in Fig. A1 indicates perforation and a negative value indicates the reflection of the projectile.

As described in Section 2.2, Lambert and Jonas relation (Lambert and Jonas, 1976):

$$V_R = a\left({V_I}^p - {V_{bl}}^p\right)^{1/p} \tag{A1}$$

was fitted to the data points with positive values of V_R for each configuration. The coincidence of this curve with the impact velocity axis is taken to be the ballistic limit. The ballistic limit and fitting parameters for all target configurations are listed in Table A1.

References

Amini, M.R., Isaacs, J., Nemat-Nasser, S, 2010. Investigation of effect of polyurea on response of steel plates to impulsive loads in direct pressure-pulse experiments. Mech. Mater. 42, 628–639.

Amini, M.R., Isaacs, J.B., Nemat-Nasser, S, 2010. Experimental investigation of response of monolithic and bilayer plates to impulsive loads. Int. J. Impact Eng. 37, 82–89.

ASTM D638-10. Standard Test Method for Tensile Properties of Plastics. 2010.

ASTM E8/E8m-11. Standard Test Methods for Tension Testing of Metallic Materials. 2011.

Atkins, A.G., Afzal khan, M., Liu, J.H, 1998. Necking and radial cracking around perforations in thin sheets at normal incidence. Int. J. Impact Eng. 21, 521–539.

Awerbuch, J., Bodner, S, 1974. Analysis of the mechanics of perforation of projectiles in metallic plates. Int. J. Solids Struct. 10, 671–684.

Backman, M.E., Goldsmith, W, 1978. The mechanics of penetration of projectiles into targets. Int. J. Eng. Sci. 16, 1–99.

Barsoum, R.G.S., Dudt, P.J, 2010. The fascinating behaviors of ordinary materials under dynamic conditions. AMMTIAC Q. 4, 11–14.

Bartczak, Z., 2005. Effect of chain entanglements on plastic deformation behavior of linear polyethylene. Macromolecules 38, 7702–7713.

Bartczak, Z., 2010. Effect of chain entanglements on plastic deformation behavior of ultra-high molecular weight polyethylene. J. Polym. Sci. Part B Polym. Phys. 48, 276–285.

Børvik, T., Langseth, M., Hopperstad, O.S., Malo, K.A, 2002. Perforation of 12 mm thick steel plates by 20 mm diameter projectiles with flat, hemispherical and conical noses. Int. J. Impact Eng. 27, 19–35.

Chen, Y., Clausen, A.H., Hopperstad, O.S., Langseth, M., 2009. Stress–strain behaviour of aluminium alloys at a wide range of strain rates. Int. J. Solids Struct. 46, 3825–3835.

Corran, R.S.J., Shadbolt, P.J., Ruiz, C, 1983. Impact loading of plates—an experimental investigation. Int. J. Impact Eng. 1, 3–22.

Gupta, N.K., Iqbal, M.A., Sekhon, G.S, 2007. Effect of projectile nose shape, impact velocity and target thickness on deformation behavior of aluminum plates. Int. J. Solids Struct. 44, 3411–3439.

Iqbal, M.A., Gupta, G., Diwakar, A., Gupta, N.K, 2010. Effect of projectile nose shape on the ballistic resistance of ductile targets. Eur. J. Mech. A/Solids 29, 683–694.

Lambert J.P., Jonas G.H. Towards Standardization in Terminal Ballistics Testing: Velocity Representation. 1976; Report BRL-R-1852.

Leppin, S., Woodward, R.L, 1986. Perforation mechanisms in thin titanium alloy targets. Int. J. Impact Eng. 4, 107–115.

Li, Y., Luo, M., Gerlach, J., Wierzbicki, T, 2010. Prediction of shear-induced fracture in sheet metal forming. J. Mater. Process Technol. 210, 1858–1869.

Liu, Y., Liaw, B, 2009. Drop-weight impact tests and finite element modeling of cast acrylic/aluminum plates. Polym. Test. 28, 808–823.

Luo, M., Wierzbicki, T, 2010. Numerical failure analysis of a stretch-bending test on dual-phase steel sheets using a phenomenological fracture model. Int. J. Solids Struct. 47, 3084–3102.

Mock W.J., Holt W., Sutherland G., Lee G., Balizer E., Fedderly J. Penetration Protection Experiments Using Polymer Materials. 2005; Technical report, Presentation by NAVSEA to ONR.

Mohagheghian I., McShane G.J., Stronge W.J. Quasi-static and impact perforation of polymer–metal bi-layer plates by a blunt indenter. Submitted for publication.

Mohagheghian, I., McShane, G.J., Stronge, W.J, 2015. Impact perforation of monolithic polyethylene plates: projectile nose shape dependence. Int. J. Impact Eng. 80, 162–176.

Onat, E., Haythornthwaite, R, 1954. The load carrying capacity of circular plates at large deflection. J. Appl. Mech. 23, 49–55.

Oosterkamp, L., Ivankovic, A., Venizelos, G, 2000. High strain rate properties of selected aluminium alloys. Mater. Sci. Eng. A 278, 225–235.

Palomby, C., Stronge, W.J, 1988. Blunt missile perforation of thin plates and shells by discing. Int. J. Impact Eng. 7, 85–100.

Radin, J., Goldsmith, W, 1988. Normal projectile penetration and perforation of layered targets. Int. J. Impact Eng. 7, 229–259.

Roland, C.M., Fragiadakis, D., Gamache, R.M, 2010. Elastomer–steel laminate armor. Compos. Struct. 92, 1059–1064.

Roland, C.M., Fragiadakis, D., Gamache, R.M., Casalini, R, 2013. Factors influencing the ballistic impact resistance of elastomer-coated metal substrates. Philos. Mag. 93, 468–477.

Simonsen, B.C., Lauridsen, L.P, 2000. Energy absorption and ductile failure in metal sheets under lateral indentation by a sphere. Int. J. Impact Eng. 24, 1017–1039.

Teng, X., Dey, S., Børvik, T., Wierzbicki, T, 2007. Protection performance of double-layered metal shields against projectile impact. J. Mech. Mater. Struct. 2, 1309–1329.

Teng, X., Wierzbicki, T., Huang, M, 2008. Ballistic resistance of double-layered armor plates. Int. J. Impact Eng. 35, 870–884.

Walley, S.M., Field, J.E, 1994. Strain rate sensitivity of polymers in compression from low to high rates. DYMAT J. 1, 211–227.

Wierzbicki, T., 1999. Petalling of plates under explosive and impact loading. Int. J. Impact Eng. 22, 935–954.

Xue, L., Mock, W.J., Belytschko, T, 2010. Penetration of DH-36 steel plates with and without polyurea coating. Mech. Mater. 42, 981–1003.

Xue, Z., Hutchinson, J.W, 2007. Neck retardation and enhanced energy absorption in metal–elastomer bilayers. Mech. Mater. 39, 473–487.